

Stony Brook University



OFFICIAL COPY

The official electronic file of this thesis or dissertation is maintained by the University Libraries on behalf of The Graduate School at Stony Brook University.

© All Rights Reserved by Author.

**An Experiment System for Studying Robotic Needle
Biopsy of Lung Nodules with Respiratory Motion**

A Thesis Presented

By

Kaarvannan Thiruvalluvan

To

The Graduate School

In Partial Fulfillment of the Requirements for the Degree of

**Master of Science
In
Mechanical Engineering**

**Stony Brook University
May 2011**

Stony Brook University

The Graduate School

Kaarvannan Thiruvalluvan

We, the thesis committee for the above candidate for the
Master of Science degree, hereby recommend
acceptance of this thesis.

Yu Zhou – Thesis Advisor

Assistant professor, Department of Mechanical Engineering

Chad Korach – Chairperson of Defense

Assistant professor, Department of Mechanical Engineering

Anurag Purwar - Member

Research assistant professor, Department of Mechanical Engineering

This thesis is accepted by the Graduate School

Lawrence Martin
Dean of the Graduate School

An Experiment System for Studying Robotic Needle Biopsy of Lung Nodules with Respiratory Motion

By

Kaarvannan Thiruvalluvan

Master of Science

in

Mechanical Engineering

Stony Brook University

2011

Abstract—this work presents the design and test of an experiment system for studying a novel CT-guided robotic needle biopsy technique. CT-guided needle biopsy is a dominant method of obtaining tissue samples from lung nodules for lung cancer diagnosis. Current practice requires patients to hold their breath during the procedure, which is not applicable to those who have difficulty in holding breath. The CT-guided robotic needle biopsy technique adapts to the patient respiratory motion pattern and uses a robot manipulator to drive the biopsy needle towards a target lung nodule with respiratory motion, which will enable biopsies on patients who have difficulty in holding breath and improve the needle placement accuracy. An offline experiment system has been created to facilitate the development and evaluation of algorithms for planning and controlling the robotic needle placement process. It consists of three subsystems coordinated by a computer, i.e. a moving lung nodule phantom subsystem which mimics a lung nodule with respiratory motion, a robotic needle manipulation subsystem which drives the biopsy

needle to hit the moving lung nodule, and a real-time vision feedback subsystem which tracks the moving lung nodule phantom to provide feedback for controlling the needle placement. The results from a sequence of needle placement tests based on clinically-obtained lung nodule motion paths show that the robotic needle placement technique has the potential to provide highly accurate needle delivery on moving nodules and allow biopsy of nodules smaller than usually considered. The bending of the needle when inserted into tissue affects the accuracy of many percutaneous procedures including the lung biopsy. This issue is traditionally tackled by additional medical imaging, which is expensive. A simple method has been derived to accurately predict the position of the needle tip. An algorithm of the new method has been developed and tested with satisfactory accuracy.

*To
Arulmalar
And
Thiruvalluvan*

Table of Contents

List of Tables	vii
List of Figures	viii
Acknowledgement	ix
Chapter 1. Introduction	1
1.1 Lung Cancer	1
1.2 CT-Guided Needle Biopsy	2
1.3 Robotic Needle Placement	4
Chapter 2. Over view of CT-Guided Robotic Needle Biopsy of Lung Nodule	6
2.1 Respiratory Motion Modeling	6
2.2 Needle Path Placement.....	7
2.3 Needle Driving	8
Chapter 3. Experiment System For Robotic Needle Biopsy Of Lung Nodules	11
3.1 Moving Lung Module Phantom Subsystem.....	12
3.2 Robotic Needle Manipulation Subsystem	16
3.3 Real-time Vision Feedback Subsystem.....	25
3.4 Coordination And Correspondence among Subsystems	31
Chapter 4. Needle Placement Tests	36
Chapter 5. Bending	45
5.1 Overview of the Needle Bending Problem	45
5.2 The Force Distribution Approximation method.....	46
5.3 Experimental Testing	49
Chapter 6. Conclusion And Future Work	59
References	62

List of Tables

Table 3.1 Speed Levels	19
Table 4.1 Motion Path Case 1	38
Table 4.2 Motion Path Case 2	39
Table 4.3 Motion Path Case 3	40

List of Figures

Figure 1.1 CT of the Lung	2
Figure 1.2 CT guided needle biopsy	3
Figure. 3.1. Experiment system for robotic	12
Figure 3.2 Fiducial Marker and the Lung Nodule Phantom	13
Figure 3.3 Lung Nodule Phantom	14
Figure 3.4 UI-600 run page	15
Figure 3.5 The Robot	16
Figure 3.6 Axes of the Robot	17
Figure 3.7 Cartesian Coordinate System	17
Figure 3.8 Structural Flags	18
Figure 3.9 RoboWare	22
Figure 3.10 Needle Gripper	23
Figure 3.11 Cross-section CT scan of the needle gripper	24
Figure 3.12 Fiducial Marker	26
Figure 3.13 Logical Image	28
Figure 3.14 Points on a 3D trajectory	29
Figure 4.1 Needle placement test	37
Figure 4.2 Displacements in Case 1	38
Figure 4.3 Displacements in Case 2	39
Figure 4.4 Displacements in Case 3	40
Figure 4.5 Needle paths	44
Figure 5.1 Cantilever Beam	46
Figure 5.2 Experimental setup	50
Figure 5.3 Data Acquisition using LabVIEW	51
Figure 5.4 Points on needle observed by using camera	52
Figure 5.5. Bent needle observed using camera	53
Figure 5.6 Bending of the needle	54
Figure 5.7 Predicted tip of the needle	54
Figure. 5.8. Force distributions curves with equations	56
Figure 5.9 Uniformly Varying Force Distribution	57
Figure 5.10 Random Force Distribution	58

Acknowledgement

I thank Professor Yu Zhou, for all his guidance and support.

I thank Dr. William H. Moore and Lukasz Krzeminski for their contributions to this project.

I thank Siva, Aarthi, Nambi and Kamal for their support and friendship.

Finally, I thank my parents and grandparents for their countless sacrifices, which have enabled me to pursue my dreams.

Chapter 1. INTRODUCTION

This thesis presents the design and test of an offline experiment system for studying a CT-guided robotic needle biopsy technique for biopsy of lung nodules with respiratory motion. The underlying research work aims at using robotic technology to adapt to the stabilized patient respiration and enable accurate and quick placement of a biopsy needle onto a moving lung nodule.

1.1 Lung Cancer

Lung cancer is the worldwide most common cause of cancer-related death in men and the second most common cause of cancer-related death in women [1], resulting in 1.3 million deaths/year [2]. In the United States, lung cancer is the largest cause of cancer-related death in both men and women, responsible for 30% of all cancer deaths [3]. An estimated 162,460 deaths from lung cancer would occur in US during 2006 [4]. Early detection is of critical importance in reducing morbidity and mortality rates in high-risk individuals who are screened for lung cancer [5,6].

Lung nodules are often detected by imaging examinations, including chest x-ray and computed tomography (CT). However, it is not always possible to tell from these imaging tests whether a lesion is benign or cancerous. Following the identification of a suspicious lesion, a sample of the suspicious tissue is removed and examined under the microscope to confirm the diagnosis. Bronchoscope, open biopsy, video-assisted thoracoscopic surgery, mediastinoscopy and needle biopsy are the commonly used biopsy techniques. A thin tube is sent to the lung through the mouth or the nose to collect the sample tissue in Bronchoscope. The patient's chest is opened to collect samples in open biopsy. In video-assisted thoracoscopic surgery, several

small holes are made; a camera is inserted into one of the holes and specialized equipments are sent into the other holes to remove a sample of the abnormal tissue. In mediastinoscopy a small tube is sent into the lung from an insertion made at the base of the neck. In needle biopsy a biopsy needle is inserted into the lung to the location of the nodule and a sample is taken out using a syringe. A needle biopsy is often performed when the nodule is unreachable by other diagnostic techniques.

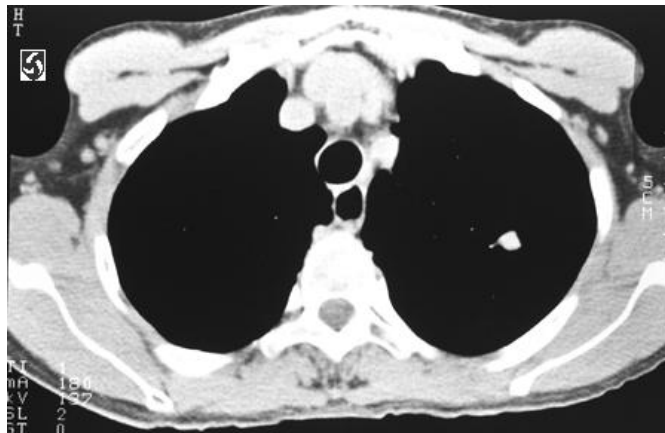


Figure 1.1 CT of the Lung

1.2 CT-Guided Needle Biopsy

CT-guided needle biopsy has become a dominant method of obtaining tissue samples from lung nodules for lung cancer diagnosis [7-32]. It needs to be performed by a specially-trained interventional radiologist. The patient will lie on a CT table, and be injected a local anesthesia to numb the needle path. The nodule will be located through a pre-operative CT scan (Figure 1.1). The safest needle path will be planned, and the entry site will be marked on the skin. The patient will be required to stay still and hold breath during the operation. Using intra-operative CT scans to confirm the positions of the nodule and needle, the clinician will insert the needle through the skin, advance it to the target nodule, and remove tissue samples. CT-guided

needle biopsy is minimally invasive, eliminating the added morbidity of open surgery and requiring no general anesthesia. The procedure is in general not painful. The patient can soon recover and resume their usual activities.

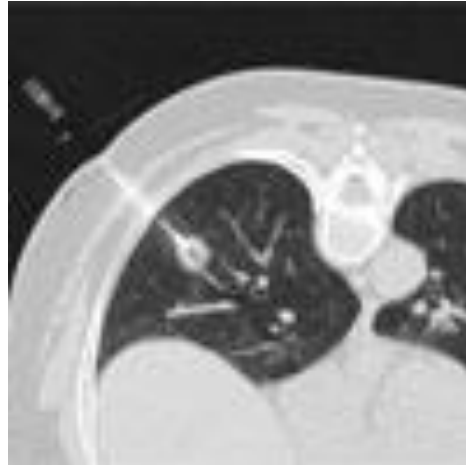


Figure 1.2 CT guided needle biopsy. [107]

The tissue sampling accuracy and patient safety are critical in the CT-guided needle biopsy of lung nodules, and impose serious challenges. Accurate needle placement depends on the clinician's skill and consistency and the patient's compliance. The nodule size and location contribute to the difficulty in needle placement. Though ideally located nodules as small as 4mm have been reported as biopsied [33], in general lesions ≤ 8 mm are very difficult to approach. The diagnostic accuracy generally decreases with smaller lesions and longer needle paths [34-36]. Moreover, for rapid, safe and accurate biopsy, it is important for the patient to remain still and repeat breath hold during needle manipulations, because a lung nodule can displace up to >20 mm during a respiratory cycle [37,38]. Thus, it is highly challenging to perform biopsies in patients who have difficulty in holding breath (about 10%-15% of our patients). Besides, the procedure duration ranges from 15 minutes to over an hour depending on CT, cytology availability, nodule accessibility and patient compliance. Long-time remaining still and holding

breath will make the patient uncomfortable and degrade the level of compliance. Inaccurate needle positioning and insufficient patient compliance may increase the number of needle passes and occurrence of complications such as pneumothorax and bleeding.

To solve the problems with the existing procedure of the CT-guided needle biopsy of lung nodules, we propose a CT-guided robotic needle placement technique which targets to 1) enable the biopsy on patients who have difficulty in holding breath, 2) improve the biopsy accuracy and reduce the biopsy duration, and thus reduce the incidence of complications and improve the patient safety.

1.3 Robotic Needle Placement

Image-guided robots have been growing as an important technological assistance to image-guided percutaneous procedures, with great potential to provide fast, accurate, stable tool placement and eliminate the radiation exposure on clinicians. Various robotic percutaneous systems have been developed or researched [39-96], guided by different imaging modalities, such as ultrasound [41,42,71-73,78,80,85,91,93-95], fluoroscopy [55,56,61,69,76], CT [39,40,43,49,59,60,68,71,75,77], CT fluoroscopy [51,58,62,76], and MRI [50,52-54,63,64,66,67,69,74,75,79,81,83,86,88-90,92,96]. These robots have been designed for stereotactic biopsy and neurosurgery [39,40,43-46,49,69], prostate biopsy and brachytherapy [41,42,47,60,63,73,79-81,84,85,88-91], percutaneous renal access [55,56], breast biopsy and therapy [50,61,64,67,74,93,94], percutaneous cholecystostomy [72], etc.

We notice that most, if not all, of the existing robotic percutaneous systems intend to provide a steady-hand assistance to the involved procedures, but depend on the clinician to control the robot motion, while image guidance provides the real-time visual feedback for tracking and controlling the tool position and orientation. Such a clinician-depending robot

control scheme has been reported sufficient for relatively static organs, such as the prostate, breast and lung under breath holding, but is highly challenging for operating on moving targets, such as a lung nodule under respiratory motion, due to the high requirement on real-time eyes-hands-mind coordination to the clinician. Thus, the clinician-operated robotic percutaneous systems would in general have difficulty in attaining high targeting accuracy and low procedure duration when dealing with moving targets. In the specific scenario of CT-guided needle biopsy of moving lung nodules, it tends to increase the number of needle passes, occurrence of complications, and radiation exposure on the patient, and degrade the patient comfort and safety. Consequently, performing percutaneous operations on moving targets requires higher agility in the underlying percutaneous systems than the currently-taken manual procedures and clinician-operated robotic percutaneous systems.

We propose to maximize the operational agility of percutaneous procedures for moving targets via high robotic autonomy. A CT-guided robotic needle biopsy technique for lung nodules is under research. An experiment system for robotic needle placement on moving targets has been developed. It is an offline system which facilitates the development and evaluation of algorithms for planning and controlling the robotic needle placement process but has not yet been integrated with CT. A sequence of preliminary tests has been conducted.

This thesis reports the design and tests of the offline experiment system. The layout of the rest of the thesis is as follows. Chapter 2 will provide an overview of the proposed CT-guided robotic needle biopsy of lung nodules. Chapter 3 will describe the composition of the offline experiment system. Chapter 4 will report the settings and results of the preliminary tests. Chapter 5 will describe the needle bending problem and the proposed solution. Chapter 6 will conclude the thesis and discuss the future work.

Chapter 2. OVERVIEW OF CT-GUIDED ROBOTIC NEEDLE BIOPSY OF LUNG NODULES

The proposed CT-guided robotic needle biopsy technique uses a robot manipulator to drive the biopsy needle towards a target lung nodule. It enables biopsies on patients who have difficulty in holding breath as well as to improve the needle placement accuracy in the breath-holding case. Targeting to biopsy lung nodules with respiratory motion, a schematic process of the CT-guided robotic needle biopsy of a lung nodule consists of the following core steps:

2.1. Respiratory motion modeling

A series of pre-operative CT scans will be performed on the patient under the free, relaxed breathing condition, from which a sequence of volumetric CT images corresponding to the patient respiratory phases will be obtained. This is known as 4DCT. The method involves taking a lot of CT scans and then assigning them to different phases of the respiration cycle. This relatively new technology is used to observe the movement of the tumor inside the lung as the patient breathes. From the phase-labeled volumetric CT images, the periodic respiratory motion model of the target lung nodule and surrounding internal structures/organs, such as the rib cage, heart, major vessels, diaphragm and mediastinum, called internal respiratory motion model, will be created. While the 4DCT is being taken a normal camera observes the movement of the fiducial marker placed on the skin. The correlation between the respiratory motion of the lung nodule and that of the skin surface will be retrieved. The correlation between the lung nodule and the skin fiducial is just temporal. So the location of the fiducial marker with respect to the nodule is not needed. The need of building such correlated respiratory motion model is to know the current respiratory phase, when the actual biopsy is being done. So in any phase of respiration the position of the nodule is known based on the observation using the 4DCT and the current

phase of respiration is known from the fiducial marker. Thus current location of the nodule can be identified based on the position of the nodule.

2.2. Needle path planning

The biopsy needle will be aligned and advanced along an optimal straight-line path to hit the target lung nodule at a planned timing. This type of straight-line needle path has been dominantly, if not unanimously, adopted by manual needle biopsy of lung nodules, and proven to be convenient in needle handling and to result in maximal operational robustness and minimal complications. Based on the internal respiratory motion model, an optimal straight-line needle path will be planned by comprehensively considering the needle travel distance under the skin, internal structures /organs, needle insertion angle, and respiratory phase. In particular, an optimal respiratory window will be chosen to gate the needle advancement within one to a couple of respiratory phases when the lung nodule is at its lowest respiratory motion speed, in order to minimize the chance of missing the target and minimize the control effort for target following. It means that the needle will be advanced only within the chosen respiratory phase(s). However, not all nodules can be reached from vertically above their positions due to presence of ribs, nerve bundles, blood vessels and other organs. The robot needs to be able to do the biopsy from inclined angles also. There are two angles of interest here. One angle along the length and one angle along the width of the patient's body. These angles can be defined by defining the point of the entry in the patient's body. The clinician carefully determines the point of entry on the patient's body. The position of this entry point is measured from the location of the nodule at the planned needle advancing respiratory phase. So in the CT image of the lung at the planned respiratory phase, the center of the nodule is considered as the origin and the planned point of entry on the outer skin surface is measured in millimeters. This information is manually entered

to the central computer by the clinician. The needle path will be from this initial point to the target nodule. For the needle to travel in this path it has to be aligned exactly along the path. This is done by rotating the needle angle two different axes.

2.3. Needle driving

The robot manipulator will move the needle to its initial pose (position and orientation) which aligns with the planned needle path and is near the corresponding skin entry site. By tracking a skin-surface fiducial using a video camera (regular or infrared), the motion state (position, velocity and respiratory phase) of the target lung nodule can be inferred from the correlation between the internal and skin-surface respiratory motions. Based on this feedback, the robot manipulator will advance the needle along the planned needle path towards the targeted meeting location with the lung nodule, gated by the chosen respiratory window.

Moreover, to ensure accurate needle placement and avoid repeated needle passes, the needle pose can be confirmed and, if necessary, adjusted intra-operatively. We suggest that the needle advancement have a pause before the needle enters the lung, and a CT scan be performed to verify if the needle is along the planned path towards the targeted meeting location with the lung nodule. If necessary, the robot manipulator will reorient the needle towards the target. After the confirmation (and reorientation), the needle will be quickly advanced to hit the target. Then the robot manipulator will release the needle immediately. A follow-up CT scan will be performed to verify if the needle has physically hit the nodule. The clinician will remove tissue samples, and then retract the needle.

Here, CT is used as the imaging tool to retrieve the respiratory motion pattern of the target lung nodule and other internal structures/organs, because the high-contrast resolution of CT results in high imaging details of both hard and soft body structures and allows better

planning of the needle path for a safe biopsy, in particular for nodules that are small and deep within the lung or located near blood vessels, airways or nerves. In fact, CT is clinically preferred for lung biopsy, compared with other imaging modalities. Ultrasound can only be used to guide the biopsy of limited, peripheral lung lesions, because the air in the lung blocks ultrasound transmission [57]. MRI currently has no major role in the diagnosis or management of lung parenchymal diseases including tumors, mainly due to its lower spatial resolution and hence lower sensitivity in detecting lung nodules than those of CT [57]. Moreover, MRI-guided needle biopsy of lung nodules is difficult to realize due to the artifact induced by the respiratory and cardiac motions, in particular when the patient has difficulty in holding breath, and the artifact produced by the metallic needle. Clinical experiences have indicated that CT is preferred for lung biopsy rather than MRI [138].

Moreover, to facilitate the autonomous control of the needle placement process, we propose to use the respiratory motion model created from the pre-operative CT imaging to plan and guide the needle placement motion, instead of using continuous CT imaging during the needle placement process. This is because the reconstruction of volumetric CT images and automatic segmentation and tracking of features in volumetric CT images is still a time-consuming process, which makes real-time CT-guided autonomous robotic needle placement an extremely challenging, if not impossible, task to achieve with the existing image processing capability. However, camera-based real-time tracking of simple artificial markers has become a mature technique. By tracking a body-surface fiducial using a camera, one can infer the motion state of the internal lung nodule and other structures according to the correlation between the internal and skin-surface respiratory motion.

In addition, relaxation medication will be given to the patient to relax and stabilize the respiration for reliable respiratory motion modeling and tracking. A local anesthesia will be injected to numb the path of the needle in order to minimize the patient's reaction to the needle insertion.

Chapter 3. EXPERIMENT SYSTEM FOR ROBOTIC NEEDLE

PLACEMENT

In order to accomplish the proposed CT-guided robotic needle biopsy technique, we have created an offline experiment system to facilitate the development and evaluation of algorithms for planning and controlling the robotic needle placement process (Fig.1). This experiment system is created to fit with the concept of the CT-guided robotic needle biopsy, and part of the system can be used in the future online biopsy system. It consists of three subsystems:

- *Moving lung nodule phantom subsystem* which mimics a lung nodule with respiratory motion,
- *Robotic needle manipulation subsystem* which drives the biopsy needle to hit the moving lung nodule,
- *Real-time vision feedback subsystem*, which tracks the moving lung nodule phantom to provide feedback for controlling the needle placement.

These subsystems are coordinated by a central computer (PC). The design and functionality of these subsystems are described in the following subsections.

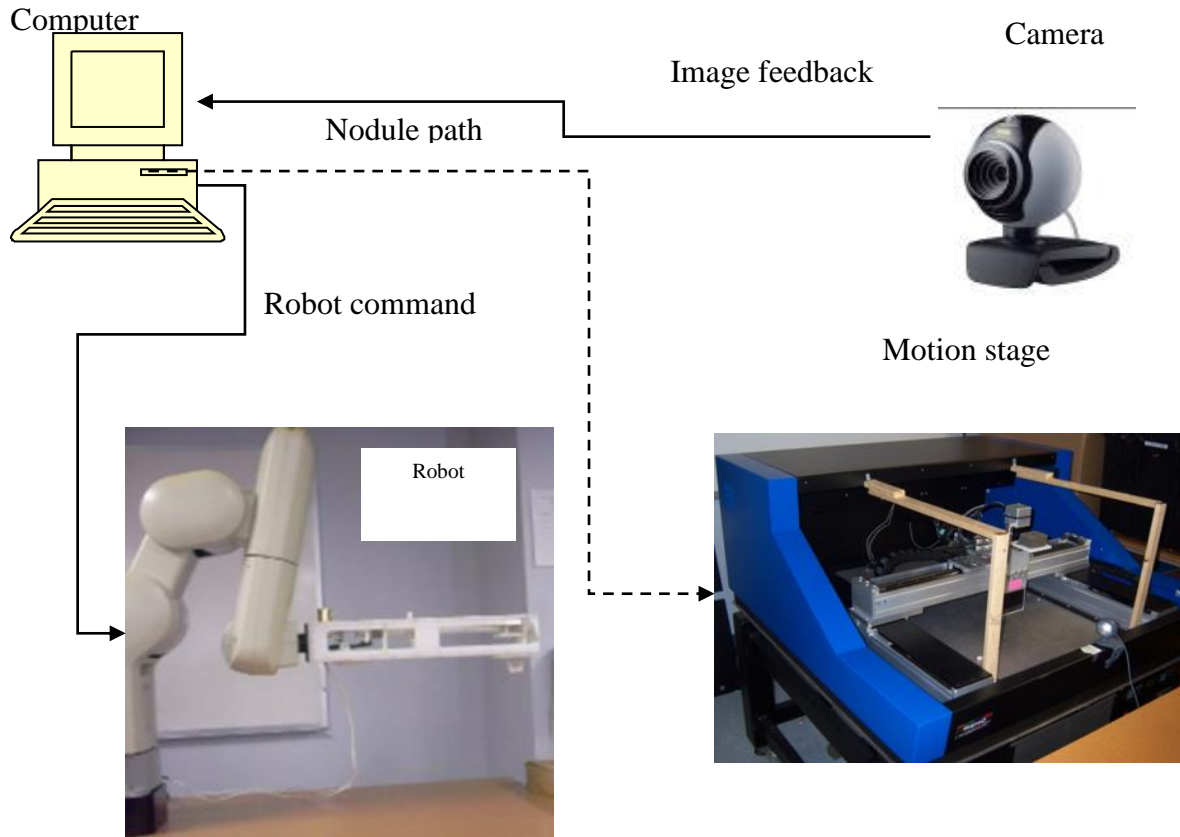


Figure. 3.1. Experiment system for robotic

3.1. Moving Lung Nodule Phantom Subsystem

This subsystem is created to mimic lung nodules with respiratory motion. A three-axis Aerotech programmable motion stage is used to simulate the movement of a target lung nodule (Figure 3.2). It allows translations in three perpendicular directions, with horizontal X and Y axes and vertical Z axis. X axis has a travel stroke of 650mm, Y axis 425mm, and Z axis 50mm, with a positioning accuracy of $\pm 5\mu\text{m}$. A static lung nodule phantom can be attached to the motion stage through a mounting bracket. The mounting bracket is fitted to the part of the motion stage that can move along all three of the axes. The motion stage and nodule phantom together mimic a moving lung nodule.

To test the positioning accuracy of robotic needle placement, a block of soft sponge

(60×55×30mm) is currently used as the lung nodule phantom to give the biopsy needle a soft target for insertion, and an ink mark on the top of the sponge represents the target point which the needle should hit and enter into (Figure 3.3). More sophisticated, other types of lung nodule phantoms will be tested later on.

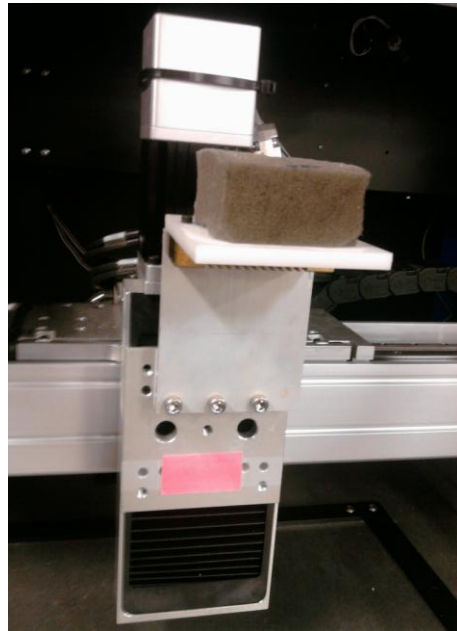


Figure 3.2 Fiducial Marker and the Lung Nodule Phantom.

The movement of the lung nodule phantom can be programmed in the Cartesian coordinate system of the motion stage using the standard G-codes and M-codes. A realistic respiratory motion trajectory of a lung nodule is translated into the corresponding motion stage codes on the central computer. The motion stage program consists of a loop of motion commands, each of which corresponds to a respiratory phase of the lung nodule motion. The program keeps repeating itself in an infinite loop until manually stopped. The program is uploaded to the motion stage controller from the central computer through an RS232 serial connection, and controls the motion stage to mimic the periodical respiratory motion of the lung nodule.

UI 600 is the software provided with the motion stage to facilitate the programming of the motion stage from a computer. The motion stage does not have enough memory to save multiple programs. It also lacks any other means of communication. So the UI 600 is the only way the motion stage can be communicated with. UI 600 has three sections, the manual jog operations section, the file handling section and the run time monitoring section (Figure 3.4).

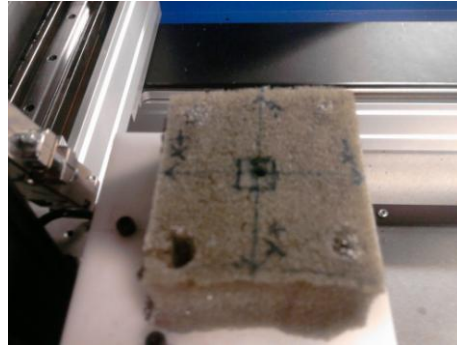


Figure 3.3 Lung Nodule Phantom.

The manual jog section enables the user to move the motion stage along its three axes manually. Homing of the motion stage can also be done using this section. The file handling section enables the user to create, save, open, find, compile and download files. Every time a motion sequence has to execute the corresponding program file is opened, compiled and downloaded to the onboard memory for execution. The run time monitoring section is activated automatically when a file is downloaded to the onboard memory. A program is held in the onboard memory till the motion stage is powered off. The run time monitoring section lets the user start, stop and pause a program. It also enables the user to step through the program line by line. The programming language used is the standard G-codes and M-codes used in CNC programming.



Figure 3.4 UI-600 run page.

Here is a sample of one of the programs used in this experiment.

DRIVE.X=1 DRIVE.Y=1 DRIVE.Z=1

G99 G70 G90

X-3 Y-2 Z0

WHILE FOREVER DO

G1 X-3.1181 Y-1.1212 Z 0.0393 F 118.9823

G1 X-3.2362 Y-0.5236 Z 0.0787F 104.4974

.

.

G1 X-3.5118 Y 1.1574Z 0.0787F 88.3374

G1 X-3.6299 Y 1.8464 Z 0.0787F 104.3321

ENDWHILE

The first line enables all the three axes. The next line sets the positioning style to absolute, makes the feed rate variable and says that multiple repetitions of the cycles are expected. Then an infinite loop is created and the points representing the different phases of the respiration are defined and the motion stage is made to move there.

3.2. Robotic Needle Manipulation Subsystem

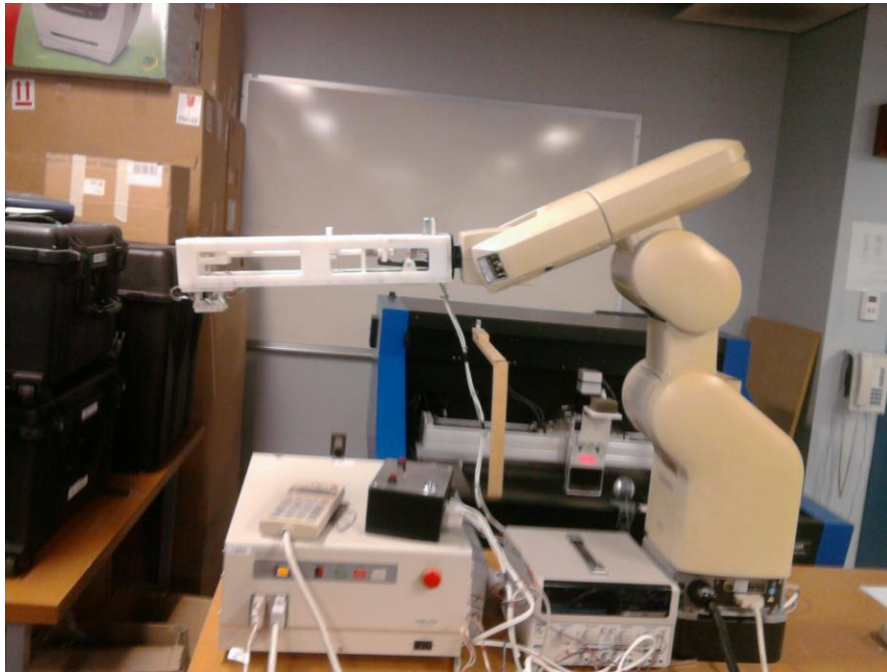


Figure 3.5 The Robot.

A Mitsubishi RV-E2 general-purpose 6-DOF articulated robot manipulator is used for needle manipulation (Figure 3.5). The robot arm has six rotational joints (Figure 3.6), and can position and move itself in both the joint space and Cartesian coordinate system (Figure 3.7). It has a position repeatability of ± 0.04 mm along X, Y and Z-axes, and a position accuracy of 0.1 mm along X, Y and Z-axes.

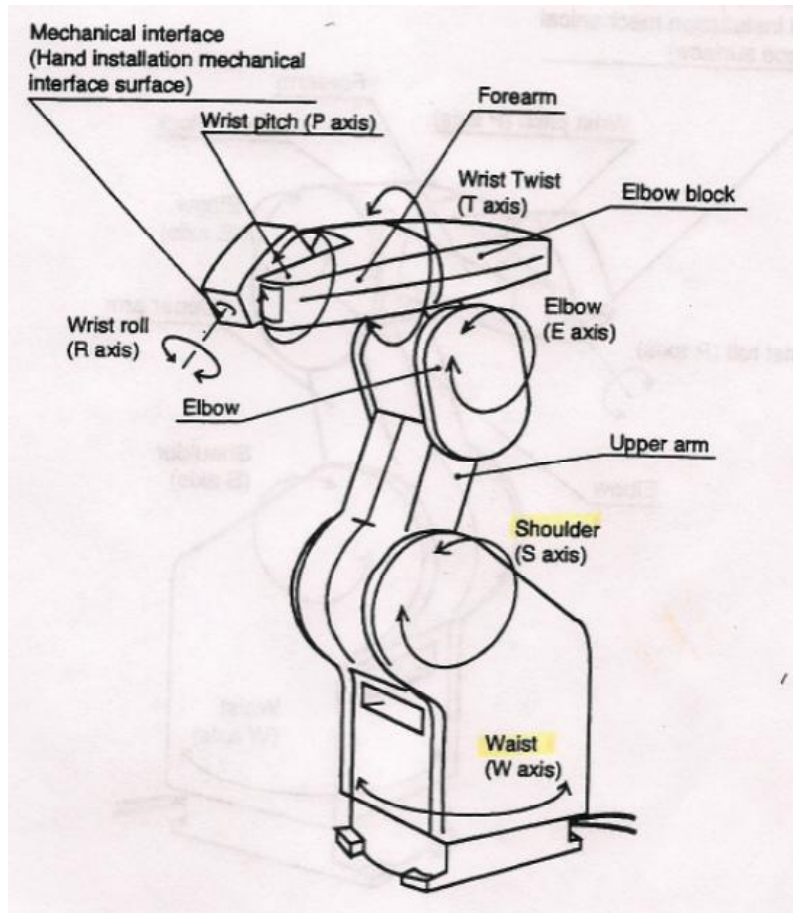


Figure 3.6 Axes of the Robot

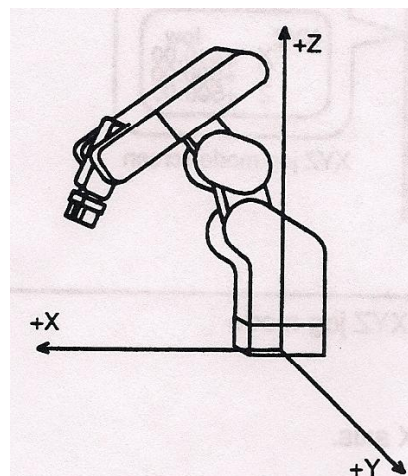


Figure 3.7 Cartesian Coordinate System

Any configuration of the robot can be specified by six angles along these axes. Linear coordinate system can also be used to specify a configuration of the robot; the robot saves positions in this fashion. Figure 3.7 explains the origin and the orientation of the XYZ frame. A typical saved position would look like this:

“PD 10,+417.69,+11.71,+304.28,+74.97,+3.38,+89.09,R,A,F,O”

“PD 10” – Position number 10 is being defined.

“+417.69,+11.71,+304.28” – defines the position of the reference point in the XYZ frame measured in mm.

“+74.97,+3.38,+89.09” – defines the orientation of the reference point i.e. the pitch, roll and the yaw angles in degrees.

“R,A,F,O” – Structure flags used to define the configuration of the robot. Figure 3.8 describes the various Structure flags.

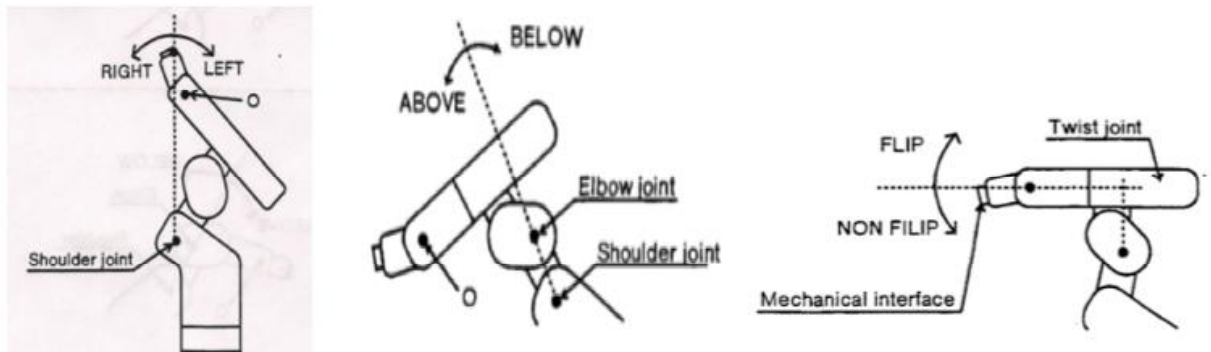


Figure 3.8 Structural Flags

The format in which these positions are saved is important because we need to use this knowledge to derive and define any new positions. In this experiment this is used to correct the initial position, i.e. the point of entry on the patient’s skin. This position is defined by the clinician with respect the position of the nodule in the planned respiratory phase. The needle may have to be aligned along two different angles to move along the axis of the needle from the initial

position to the final position. However it is to be noted that the saved position does not denote the position of the tip of the needle, instead it denotes the intersection of the wrist roll axis R and the mounting flange on which a custom made needle gripper is mounted. So the movement of the needle tip caused by aligning the needles to the planned needle path is not reflected on the saved position. This has to be manually corrected and the initial position has to be redefined.

The speed of the robot can be defined in degree/second or mm/second, depending on the type of interpolation being used. The speed of the robot is the speed of the tool tip, in our case the needle, in the XYZ coordinate frame. From rest the robot accelerates to the desired speed and retains the speed until a certain point, when it starts to decelerate. The acceleration and deceleration factors can also be adjusted. These factors are measured in terms of time, i.e. the time taken to reach the desired speed. The speed of the robot can be defined in terms of speed levels or direct measurement of mm/second. Few of the speed levels available are listed in the Table 3.1. The maximum programmable linear speed of the end-effector is 650mm/s.

Speed Level	Joint interpolation (% of total speed)	Linear interpolation (mm/second)
0	0.1	0.2
1	0.4	2.7
5	1.5	9.8
10	6.5	42.2
15	16.2	105.2
20	34.2	222.0
25	67.1	436.0
30	100	650.0

Table 3.1 Speed Levels

A dedicated control unit controls the robot. The control unit has the memory and the processor to control the robot. It has keys to start, stop and reset a program. It also has an emergency stop button, alarm reset and a small digital display. Any problematic or erroneous execution will result in an alarm sounding. The digital display will indicate a four-digit alarm code, which indicates the reason for the alarm. The alarm could be reset using the teaching box or directly from the control unit. A log of the error can be saved to the computer. However, while executing a program the occurrence of an error will not stop the execution of the program. It has to be done manually. There are emergency stop buttons in the main robot control unit as well as on the teaching box. Pressing the emergency stop button stops the power flow to all the motors in the robot and triggers an alarm. The emergency stop button has to be used with caution. The robotic arm might collapse when the emergency stop is pushed. This is because of the added weight of the custom made needle gripper. The gripper holding the needle will collapse every time the emergency stop button is pushed. The needle being the first point of contact when the gripper collapses, it bends or breaks. So the emergency stop button is avoided unless absolutely required.

The memory in the control unit is used to save programs and position data. It can save up to 9999 positions. All positions can be backed up to the computer, as position tables. These position tables can be loaded back into the control unit. The same position number could have different positions in different position tables. So it is important to load the appropriate position table needed for a particular program. All position tables might not use all the 9999 positions available. If the current position table does not define a particular position number, the previously saved position definition for that position number will be retained. Reference to a totally undefined position number will result in an alarm. This position data is battery backed up. So they do not vanish when the power is turned on. The positions are

explicitly cleared before a new position table is uploaded. This ensures that only positions defined in the position table are present in the memory of the control unit.

The control unit has analog input and output capabilities. It also has serial and parallel communication capabilities. The teaching box or a personal computer can be used to program the control unit. Both these methods use serial communication methods to communicate with the control unit. The Teaching box uses the RS422 port and the computer uses the RS232 port. The teaching box has keys to jog and program the robot. It is the simplest way to communicate with the robot. The computer is more complex and has more functionality than the teaching box. The computer becomes handy when the programs are longer than, just a few lines. The standard printer port (IEEE 1284) is available at the back of the robot control unit. It is interfaced with the custom needle gripper. The output from a single pin is wired to the gripper's control box. This output is used for programmatic control of the needle release. The particular pin is set to high in order to trigger the solenoid that releases the needle.

RoboWare, the specialized software provided with the robot, is used to communicate with the robot controller. RoboWare is the programming and control software for Mitsubishi robots (Figure 3.9). RoboWare is used in this experiment to define, save and upload positions. The Command Entry Window allows the user to type a command and executes it instantly. Programs can be entered into the editor window. RoboWare also allows the user to execute programs one step at a time. RoboWare facilitates saving programs and positions from the control unit to the computer and upload programs and position tables to the control unit. Though RoboWare is very convenient to communicate with the robot it is used only in the initial setup stage of the experiment.

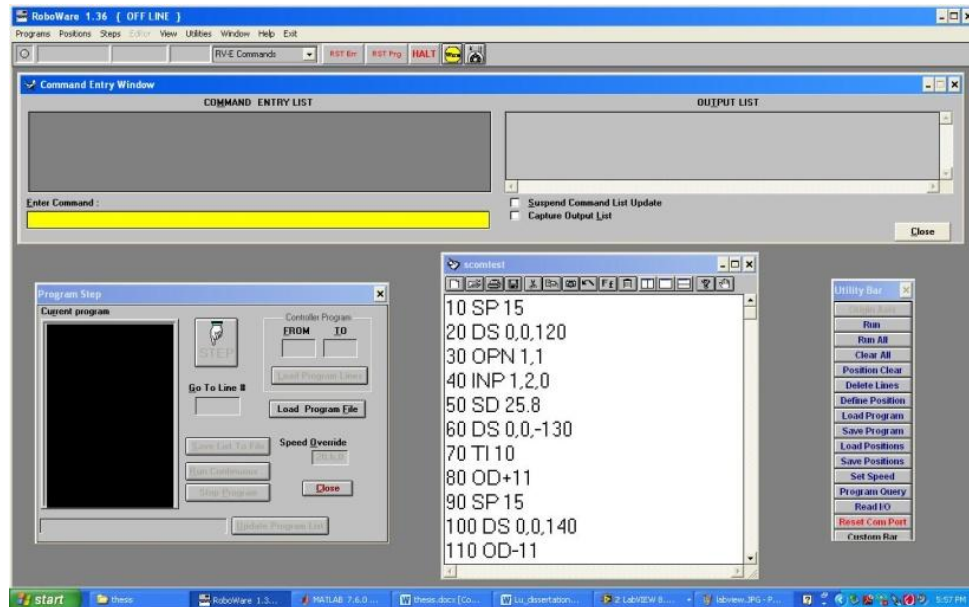


Figure 3.9 RoboWare

The robot is programmed using a custom assembly language. This assembly language uses mnemonic codes. A typical mnemonic code includes two alphabets that indicate the operation the code will perform, followed by a space and input variables to that operation. The number and format of the input variables depend on the particular mnemonic. Comma is used as the separator between the each of the inputs. Any change in format of the mnemonic will result in an error. The entire library of functions available in this assembly language is documented in the robots manual. These mnemonics are typed into the central computer using RoboWare.

Though the robot controller can save a whole control program onboard and execute it on its own, it has very limited onboard computation ability and I/O ability to interface with other devices, and consequently has limited capability of managing the control flow. To enable adaptive control of the robot, we let the central computer manage the control flow for the robot and let the robot controller work in a single-command mode. That is, the central computer sends the robot control commands one by one to the robot controller through the RS232 connection, while the robot controller executes each command immediately upon receiving it. The strong

capabilities of computation and interfacing of the central computer allow better integration between the robot and other subsystems and sensors, which leads to more flexible and robust robot control.

In the context of robotic needle placement, the main body of the robot control program consists of a sequence of motion commands, each of which advances the biopsy needle one step along the planned needle path at a designated speed in the robot Cartesian frame. Based on the camera feedback (discussed in detail in Chapter 3), the central computer will judge if the target lung nodule is in the planned needle-advancing respiratory phase(s). If yes, the computer will send next motion command to the robot controller to advance the needle; if no, no motion command will be sent. In this way, the needle placement process is gated by the planned respiratory phase. At the end of the motion sequence, the computer sends a command to the robot controller to trigger the needle gripper to release the needle.

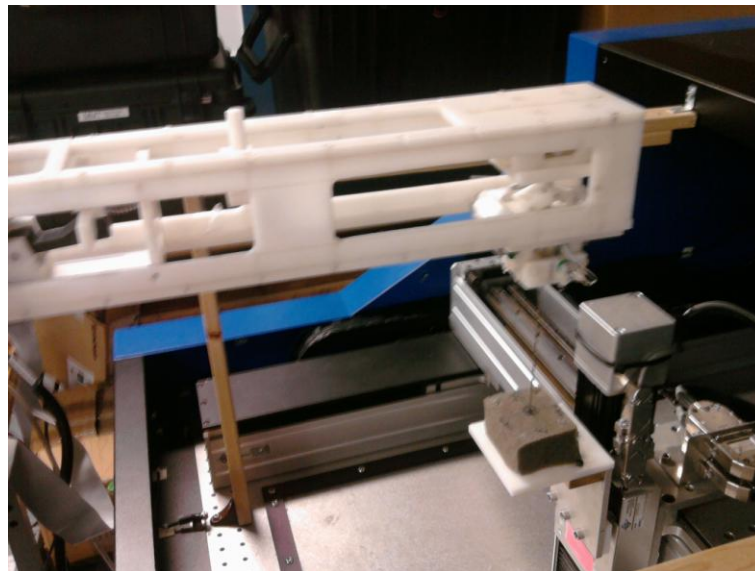


Figure 3.10 Needle Gripper

Due to the necessity of registration between robot and CT frame and online adjustment under CT guidance, the robot arm will inevitably work under CT imaging. If the robot arm is

used inside the CT bore directly, its metallic nature will cause serious deterioration in CT images, which will affect the accuracy of image processing. To solve this problem, we have designed and prototyped a CT-compatible needle gripper (Figure 3.10), which will hold the biopsy needle during the needle placement process. The needle gripper is installed on the robot arm as the end-effector. The body and mechanism of the needle gripper are made of FDA-approved plastic material Acetal. The needle gripper has an effective length of 1.5feet, which will be the only robot part operating inside the CT bore during the needle placement process. With a few small sensors and wires as the only metal pieces in the range of the CT bore (the actuator of the needle gripper will stay outside the CT bore), the metallic interference on CT imaging will be minimized (Figure 3.11). The needle gripper holds the needle tightly during the needle driving process, and releases the needle immediately after the needle is delivered to the target position.

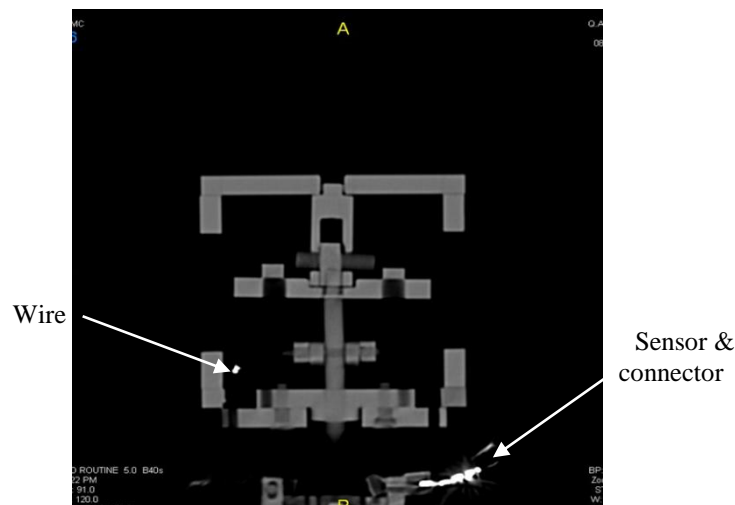


Figure 3.11 Cross-section CT scan of the needle gripper

Moreover, considering the patient safety, an emergency needle release function is added. Pressure sensors are attached to the needle gripper to monitor the forces acting on the needle in real time. If the needle is under a seriously imbalanced force distribution, such as when the

patient suddenly makes a strong cough or a large body movement, the gripper will release the needle immediately to protect the patient from serious injury. This protection mechanism also works when the force imbalance tends to cause large needle deflection. Releasing the needle will abort the procedure which could cause very inaccurate needle placement.

The needle gripper has its own control unit which interfaces with the robot controller. When the needle is delivered to the target position, the robot controller will send a signal (as the outcome of a robot control I/O command) to the gripper controller to trigger the needle release. Moreover, the above-mentioned emergency needle release function is accomplished by constantly monitoring force feedback from the pressure sensors and reactively triggering needle release by the gripper controller itself based on the detected force imbalance.

Currently a part of the offline robotic needle placement experiment system, the robotic needle manipulation subsystem described above is indeed designed for use in the realistic CT-guided robotic needle biopsy scenario.

3.3. Real-time Vision Feedback Subsystem

This subsystem is created to simulate the online tracking process of a moving lung nodule. In the proposed CT-guided robotic needle placement process (Chapter 2), the skin-surface fiducial will be tracked using a video camera, and the motion of the target lung nodule will be inferred based on the modeled correlation between the respiratory motion of the body surface and that of the lung nodule.

Currently in the experiment system, we do not physically separate the motion of the fiducial (a visual marker) and that of the lung nodule phantom. Instead, we attach a visual marker to the nodule phantom such that they move together. A fluorescent pink-colored rectangular marker (50×25mm) is attached to the fixture of the lung nodule phantom (Figure 3.12). The

bright color helps to distinguish the marker from the background. In this marker-nodule configuration, the correlation between the marker motion and the nodule motion is defined by the spatial offset between the marker and the nodule phantom. As a next step of our research, we will physically separate the marker and the nodule phantom such that they can have different but correlated trajectories.

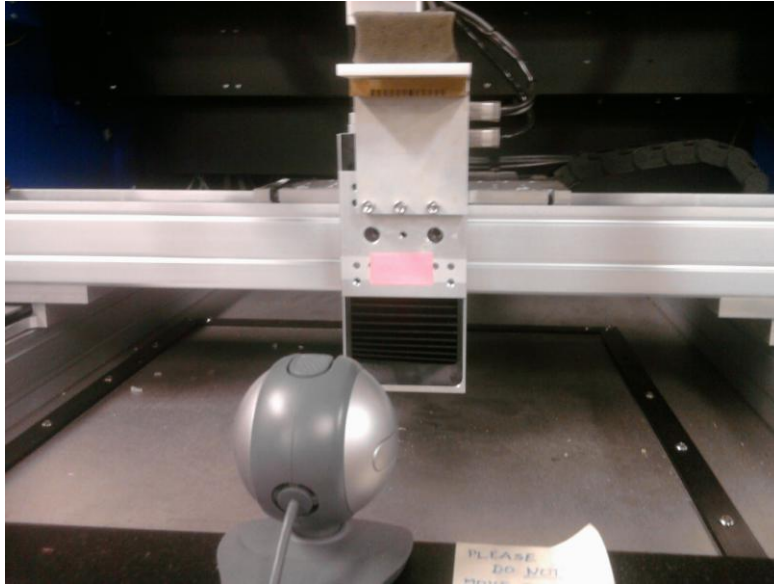


Figure 3.12 Fiducial Marker

A video camera is used to capture the moving marker, fixed relative to frames of the motion stage and robot. The Logitech C250 webcam is currently used, which has a resolution of 640×480 pixels and can capture 30 frames per second. It is set up such that the entire motion path of the marker falls into its field of view. The camera connects to the central computer via a USB connection. Whenever triggered, the camera returns an RGB color image to the computer.

The central computer processes the image to determine the position of the lung nodule phantom. The captured frame is chopped at the sides to remove unwanted pixels. The frame is chopped such that the top left hand corner of the fiducial marker is always within the frame. This chopping reduces the load on image processing thus help keeping the feedback real-time. The

image processing algorithm has to process each pixel of each frame, so chopping the image reduced the number of pixels the algorithm has to process, thus reducing the computing load. This chopping operation will be unnecessary if we can place the camera where the entire field of view is necessary, thus increasing the accuracy of the visual feedback or by increasing the processing power of the computer. The color marker is segmented from the image using a simple filter based on the corresponding pixel intensity threshold. The color marker is segmented from the image using a simple filter based on the corresponding pixel intensity threshold (Figure 3.13). The result is a logical image, with ones indicating the presence of the fiducial marker and zeros indicating the absence of the fiducial marker. Visualization of the logical image is black and white, with the white region showing the marker. Due to variable lighting conditions there might be few stray pixels in the logical image. These stray pixels are removed by a morphological operation on the image. The morphological operation being used in this experiment is 'majority'. For any given pixel its 3-by-3 neighborhood is considered. If five or more pixels in that neighborhood are one, the pixel under consideration is set to one otherwise it is set to zero. After completion of this operation, stray pixels which are false positives that have shown up due to error will be removed. The position of the marker needs to be found. In this experiment the position of the marker in the image frame is represented by the position of its top left corner. The centroid of the marker could also be chosen as the reference for the location of the marker.

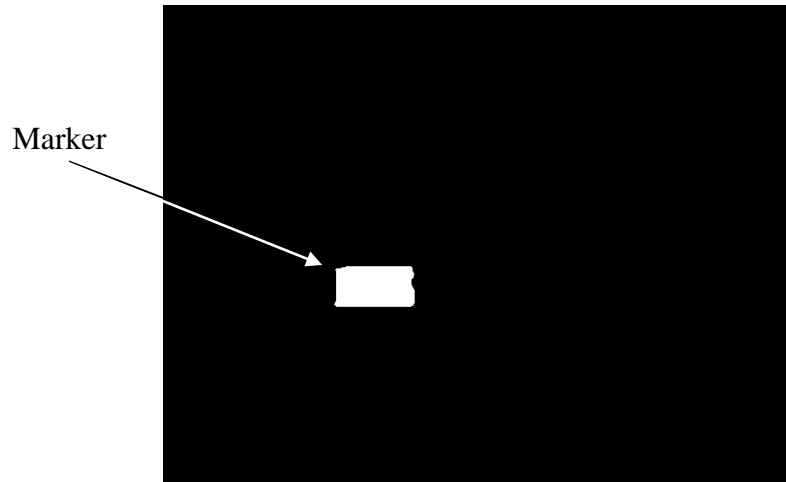


Figure 3.13 Logical Image

Observing a 3D trajectory using a 2D camera, there is a loss of dimension. So, the marker at two different locations varying only in the third dimension will look similar in the logical image except for their size. If the centroid had been chosen these two different locations would have been represented by the same point. To avoid this confusion the top left corner of the marker is chosen to represent its location. Additionally since we already know the motion sequence of the marker, we can use this knowledge to determine the exact respiratory phase. Considering the typical nodule path, two points varying only along the third dimension will have two different respiratory phases preceding them. Thus have two different locations preceding the current ambiguous location. So if the trail of the marker or the path in which the marker had moved to get to the ambiguous location is considered this problem due to loss of dimension can be avoided. The location of the marker at any given time is saved and it is retrieved to find the previous respiratory phase whenever required. The moving direction of the marker is retrieved based on the sequence of saved locations.

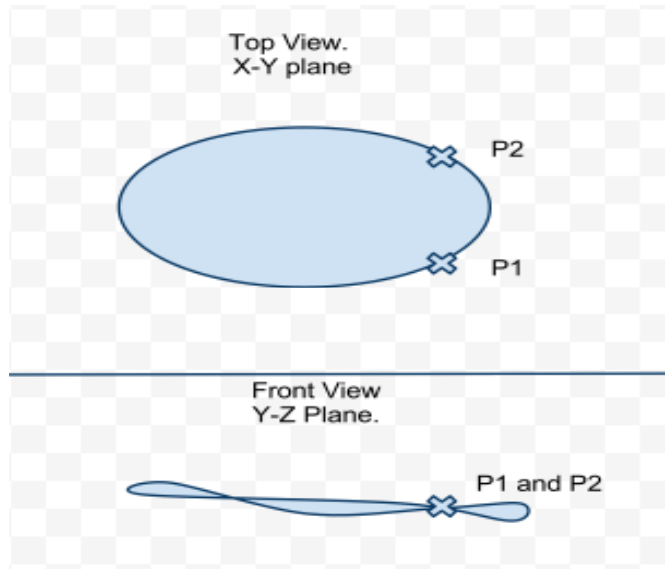


Figure 3.14 Points on a 3D trajectory

Figure 3.14 shows the top view and the front view of a random 3D trajectory. The points P1 and P2 are clearly distinguishable in the top view. However in the front view they are not distinguishable. In our experiment the camera can only see the front view, so there has to be a way by which we can distinguish points P1 and P2, which is done by considering a sequence of nodule locations leading up to the ambiguous point.

At each moment, the computer determines the current respiratory phase according to the current marker position and moving direction, by referring to the given lung nodule trajectory. In this experiment the needle is advanced only during a particular respiratory phase. The respiratory path is divided into ten phases and the location of the nodule is saved for each phase in the 4DCT described earlier. The total time taken for each cycle, that is from phase 0 to phase 9 is four seconds. So each phase lasts for 0.4 seconds. And the on observing the saved locations we can see that the points are not equidistant from each other. So the movements between the points have varying speeds. The ideal respiratory phase to advance the robot towards the target is when the movement of the tumor is at its slowest. This phase is identified after the movement of the

fiducial is observed for a certain amount of time. The numbers indicating the location of the marker are saved during the observation stage. The observation stage should be long enough to have at least one complete respiratory cycle. When the observatory stage is over, the saved locations are examined. Due to slow speed moving nature of the tumor when compared to number of frames per second the camera is capturing, there will be more than one frame with the same marker location. So finding that marker location that has been repeated the most gives the phase where the motion is at its slowest. This can be simple achieved by finding the mode of the array formed by the saved marker locations from the observation stage. Once the optimal respiratory phase to advance the robot is identified, the pixel coordinates of the fiducial while in this respiratory phase are saved. The biopsy needle is only advanced in the planned respiratory phase(s), which is known as gated needle advancement. When the marker is detected as inside the planned respiratory phase, the computer will send a command to the robot controller to advance the needle for one step, and retrieve next frame of image once the commanded motion step is finished; when the marker is detected as outside the planned respiratory phase, the computer will stop sending motion commands to the robot controller, and retrieve images at the rate of image processing. Our current version of image processing program can process about 21 frames per second, which is sufficient for real-time visual feedback. The following algorithm summarizes the image processing process:

- Step 1: Define the image acquisition object.
- Step 2: Trigger the camera and grab a frame.
- Step 3: Chop the frame to reduce image processing load.
- Step 4: Threshold the image to get a logical image.
- Step 5: Find the location of the fiducial marker.

Step 6: Compare the location of the marker with the saved location from the planned respiratory phase.

Step 7: If the current location and the planned location match send a signal to the robot. Else go to Step 2.

3.4. Coordination and Correspondence among Subsystems

The visual feedback subsystem and the robotic needle manipulation subsystem, work together, to control the needle placement process. Moreover, to facilitate robot control, all the relevant translational and rotational quantities need to be transformed into the robot frame. We recognize that there are at least three frames of reference involved in the CT-guided robotic needle biopsy process:

- 1) 3D robot frame in which the robot motion is defined (in the unit of mm),
- 2) 3D CT frame in which the respiratory motion of the target lung nodule, internal organs/structures and skin surface is modeled (in the unit of mm),
- 3) 2D camera image frame in which the skin-surface fiducial is tracked (in the unit of pixels).

The registration among these frames is of critical importance to the CT-guided robotic needle biopsy process, because the needle path and control commands are defined in the robot frame while the respiratory motion model is defined in the CT frame and the fiducial is tracked in the camera image frame.

In particular, in order to plan and control the needle trajectory in the robot frame based on the lung nodule motion in the CT frame, the transformation from the CT frame to the robot frame needs to be known. To figure out the transformation between the robot frame and CT frame ${}^{robot}_{CT}\mathbf{T}$, we can let the CT observe a CT-compatible fiducial attached to the robot (on the CT-compatible needle gripper) at a few well-defined robot configurations. Denoting ${}^{CT}_{fiducial}\mathbf{T}$ as the

homogeneous transformation representing the i 'th observed pose of the fiducial defined in the CT frame and ${}^{robot}_{fid}T_i$ that correspondingly defined in the robot frame, we in principle have

${}^{robot}_{CT}T = {}^{robot}_{fid_cr}T_i ({}^{CT}_{fid_cr}T_i)^{-1}$. A more robust estimation of ${}^{robot}_{CT}T$ can be obtained from a least-squares fitting among the pairs of ${}^{CT}_{fid}T_i$ and ${}^{robot}_{fid}T_i$ for all i .

During the needle placement process, the correspondence between the CT frame and the camera image frame is mainly used to determine the respiratory phase of the target lung nodule, in order to gate the needle advancement. This correspondence can be calibrated during the respiratory motion modeling process. While the pre-operative CT scanning records the respiratory motion path of the target lung nodule, the camera simultaneously records the correlated motion path of the (CT-compatible) skin-surface fiducial. Based on the temporal synchronization between the CT and camera imaging, the nodule motion defined in the CT frame is correlated to the skin-surface fiducial motion defined in the camera image frame. Meanwhile, the corresponding respiratory phases can be defined based on the nodule/fiducial positions and the detection of peak inhalation and exhalation, and labeled onto the motion paths of the nodule and fiducial. Thus, during the needle placement process, the respiratory phase at each moment can be found by locating the current fiducial position on the fiducial motion path in the camera image frame, and the current position of the lung nodule in the CT frame can be found based on the correlation between the nodule path in the CT frame and the fiducial path in the camera image frame.

In the current offline robotic needle biopsy experiment system, the moving lung nodule phantom subsystem mimics the respiratory motion of the moving lung nodule, which takes the place of the CT system in the real CT-guided needle biopsy process. Therefore, instead of seeking the correspondence between the CT frame and the camera image frame, we need to

figure out the correspondence between the motion stage frame and the camera image frame. In this experiment this need not be done since the interaction between the motion stage frame and the robots frame is at only one point and the position of this point is known. The point of interaction between the motion stage frame and the robot frame is at the little ink mark at the center of the sponge that acts as the lung nodule phantom, when the motion stage is at the slowest respiratory phase. So if the location of this point is known in the robot coordinate frame and the corresponding fiducial marker location is known in the camera's pixel coordinate frame we need not know the whole transformation between the robots coordinate frame and the motion stage coordinate frame. To find the location of these two points, first the slowest respiratory phase is manually found out. The motion stage is made to move to this slowest phase and paused. The needle is mounted to the gripper and the needle is aligned vertically. The robot is manually moved to the center of the sponge such that the tip of the needle pierces the ink mark made at the center of the sponge. When the robot remains in this position the current position of the robot is saved to the computer. So later when the real time tracking begins, the robot can be asked to move towards this saved point when the marker is at the planned respiratory phase. On one side, we have the knowledge of the lung nodule motion path as the input to the motion stage; on the other side, we use the camera to record the correlated motion path of the color marker (Chapter 3). Based on the temporal correspondence between the motion stage and camera imaging, the correlation between the marker motion in the camera image frame and the nodule motion in the motion stage frame is established. Thus, during the needle placement process, the respiratory phase at each moment can be found by locating the current marker position on the marker motion path in the camera image frame.

The process of controlling this whole biopsy is programmed in Matlab. Matlab provided the flexibility to control the robot and the camera from the same program. Both the camera and the robot are connected to the computer using its USB ports. They are identified in Matlab as objects. The camera object is defined by specifying the drivers to be used, the resolution, the frames per second needed to be captured when triggered and the type of trigger to expect. Once defined the object can be trigger, resulting in the 640 x 480 x 3 array of numbers. The robots serial communication port RS232 is connected to a serial to USB conversion cable and then connected to the computer. The robot is defined as a serial communication object. The baud rate and the terminators are also defined. These serial communication specifications defined has to match the serial communication specifications of the robots control unit. Once the object is defined and initialized the robots controller listens to only Matlab until the object is closed. So Matlab and RoboWare cannot function at the same time.

As a summary of the discussions on control and feedback in previous subsections, the general control flow of the biopsy needle placement process is shown in Figure 3.15.

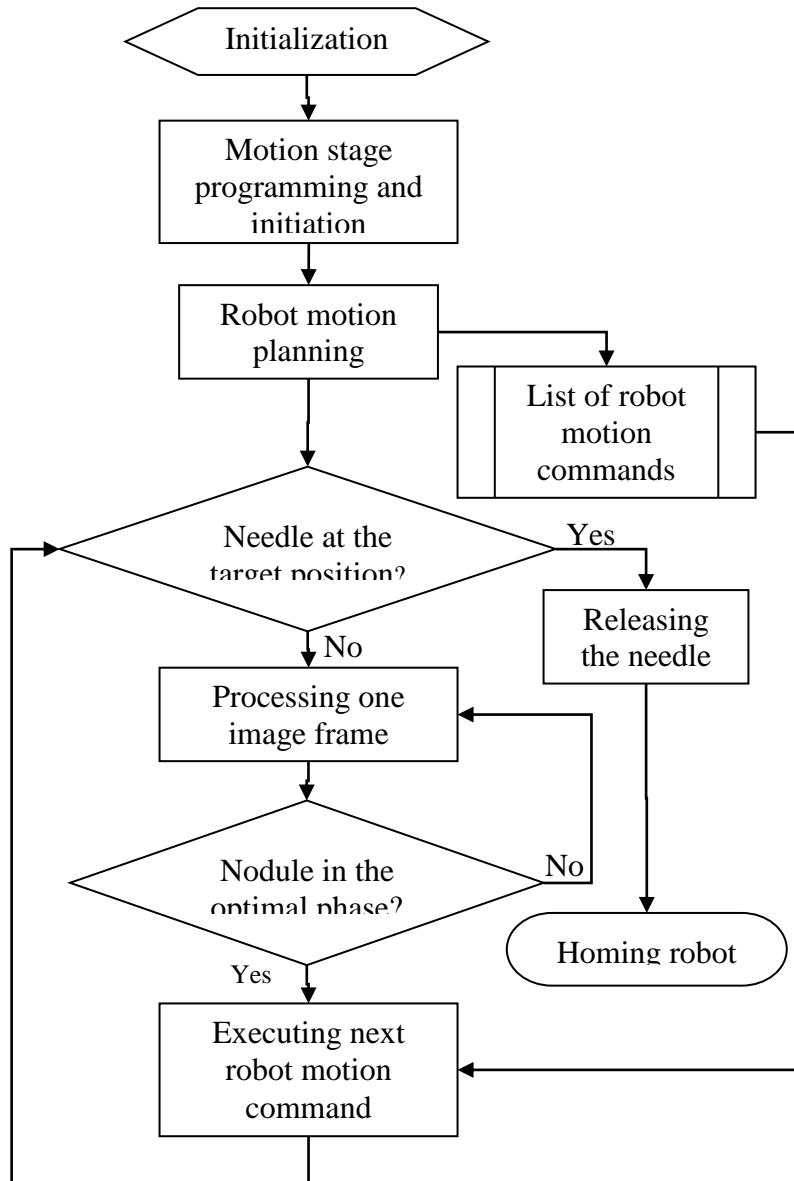


Figure 3.15 System control flow

Chapter 4. NEEDLE PLACEMENT TESTS

Preliminary tests have been conducted using the above experiment system to verify the effectiveness of robotic needle placement.

The process of each test in general follows the control flow shown in Figure 3.15. Basically,

- 1) The motion stage is programmed to simulate the respiratory motion of a lung nodule, with a soft sponge block attached as the physical target, an ink mark on the top surface of the sponge indicating the target point where the needle will hit and insert, and a color marker attached for visual tracking.
- 2) The user is asked to enter the initial position to plan a needle path. The initial position would be the point of entry in the patient's body. In this experiment it used merely to define the needle alignment angles.
- 3) A straight-line needle path is planned corresponding to the lung nodule trajectory, with the goal of hitting the target point on the moving nodule phantom at an optimal respiratory phase in which the nodule is at its lowest speed.
- 4) The robot moves the needle from the home position to the initial position, aligns it along the planned needle path, and stands by.
- 5) The central computer triggers the camera to track the motion of the color marker and estimates the instantaneous respiratory phase in which the lung nodule phantom is.
- 6) Once the lung nodule phantom moves into the planned needle-advancing respiratory phase, the computer commands the robot to swiftly advance the needle along the planned needle path to plunge into the target point (Figure 4.1), then release the needle, and finally move back to

its homing configuration.

After each test, the needle placement error is measured as the distance between the actual needle entry point and the ink mark on the sponge.

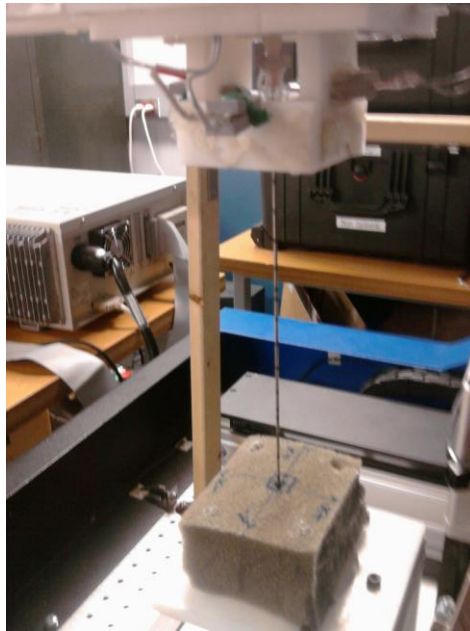


Figure 4.1 Needle placement test

To test the capability of the proposed robotic needle placement technique in dealing with real lung nodule motion paths, three representative clinically-obtained lung nodule motion paths are mimicked in our tests. Table 4.1 provides the data of these lung nodule motion paths, while Fig.10 provides the corresponding graphs. These data were taken by a 4DCT system (so X, Y and Z matches the three axes of the CT frame).

Case 1		Displacement (mm)	
Phase	X (LT/RT)	Y (Ant/Post)	Z (Inf/Sup)
0	-4.9	0	27.5
10	-4.9	1	22.5
20	-3	0	17.5
30	-2	0	10
40	0.9	0	5
50	0	0	0
60	0.9	1	-2.5
70	-4.9	1	0
80	-4.9	1	2
90	-4.9	1	10

Table 4.1 Motion Path Case 1

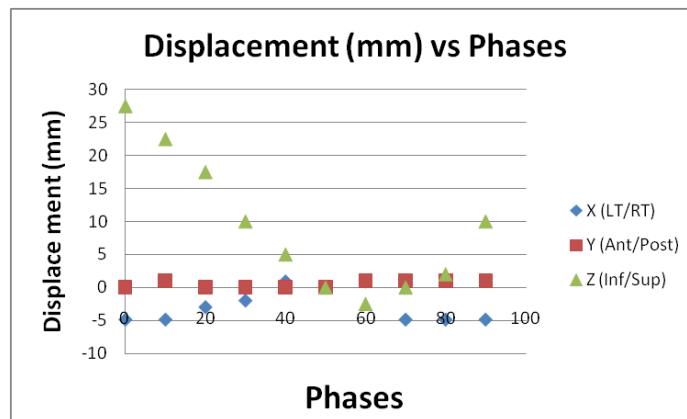


Figure 4.2 Displacements in Case 1

Each set of data represents a periodic respiratory motion path of a lung nodule. A respiratory cycle, which typically takes 4 seconds, is equally divided into 10 phases. After the 10th phase, the 1st phase follows, and the cycle repeats itself. The 3D position of the lung nodule at each phase is given. Table 4.1 shows some typical respiratory motion ranges, from 10mm to 20mm. The speed of a lung nodule varies from phase to phase. There are phases where the nodule speed becomes very low or even zero, such as Phase 50 in every case of Table 4.1 which corresponds to full exhalation. These are the ideal phases to advance the needle to hit the target. In our experiment system, to mimic the lung nodule respiratory motion with the motion stage,

the nodule displacements in X, Y and Z directions of the CT frame are mapped to the displacements in Y, Z and X directions of the motion stage frame respectively.

Case 2		Displacement (mm)	
Phase	X (LT/RT)	Y (Ant/Post)	Z (Inf/Sup)
0	-3	1	12.5
10	-3	1	12.5
20	-1	0	7.5
30	-1	0	5
40	0	0	0
50	0	0	0
60	-1	0	2.5
70	-3	0	5
80	-1	0	10
90	-3	0	15

Table 4.2 Motion Path Case 2

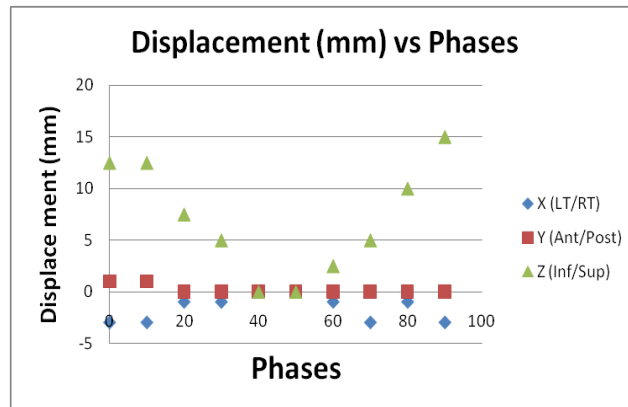


Figure 4.3 Displacements in Case 2

Case 3		Displacement (mm)	
Phase	X (LT/RT)	Y (Ant/Post)	Z (Inf/Sup)
0	-3	1	20
10	-3	1	17.5
20	-1	0	10.1
30	-1	0	2.5
40	0	0	2.5
50	0	0	0
60	-1	0	2.5
70	-3	0	10.1
80	-1	0	15
90	-3	0	17.5

Table 4.3 Motion Path Case 3

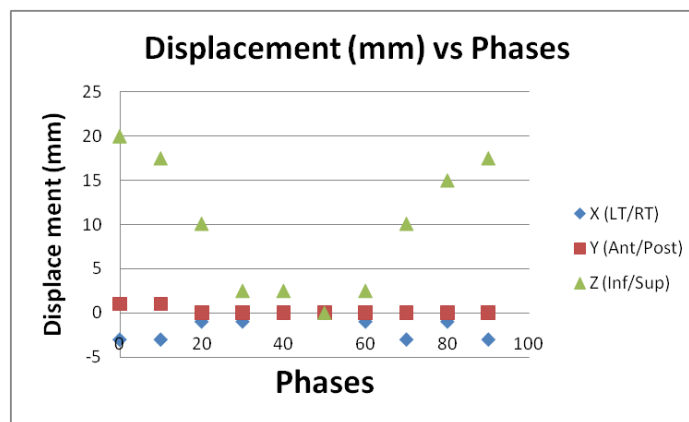


Figure 4.4 Displacements in Case 3

In this path the nodule remains without moving for phase consecutive phases. Thus it adds up to 0.8 seconds of inactivity. This provides a longer window in which the nodule could be hit. Also the maximum displacement of the nodule is also smaller when compared to the previous path. Table 4.3 shows the third motion path that was used for testing. Similar to the first motion path it also has a 0.4 second window in which the nodule should be hit. The maximum displacement is smaller than in the first motion path.

The input of the user is in millimeters denoting the initial position with reference to the nodule position at the planned respiratory phase. This input is used to calculate the angles by which the needle must turn in order to align itself to the needle advancement path. This is very

important because even a small difference between the needle alignment angle and the needle path will result in needle bending and will hurt the patient. The angles by which the needle needs to turn are calculated based on basic trigonometry. The length and height of the gripper are to be known to make these calculations.

The relation between the saved robot configuration and the position of the needle tip will change as soon as the needle is aligned. We do not know the complete transformation of that connects the robots coordinate system to the motion stages coordinate system. So this change in relation between the saved position and the needle tip position has to be countered manually. This is done by finding the difference in motion stage coordinates, that the change in alignment of the needle has caused. Once this difference is found, the saved target position has to be adjusted. The target position would have been saved in the robot control unit during the preparatory phases. This position is retrieved to the central computer. The position data will be string of characters. This string is broken down into smaller strings separated by commas. Then the smaller strings are converted into number. These numbers are changed to reflect the change in the relation between the saved robot configuration and the needle tip position. All the altered values are concatenated to form a complete position string and this string is sent back to the controller and executed. Thus the target position will be redefined. The algorithm that is being used is unstable, meaning it can fail if a new target position far away from the current target position is chosen. However as far as this experiment is concerned the algorithm will be effective since there is only one target position. This can be avoided if the complete transformation between the robots coordinate frame and the motion stages coordinate frame is known. The target will be saved in the motion stage coordinate frame instead of the robots coordinate frame.

The saved robot configuration can then translated to a point on the motion stage coordinate frame, thus avoiding the need for these string manipulations.

Based on these lung nodule respiratory motion paths, 150 different straight-line needle paths are planned to test the needle placement from different directions relative to the nodule motion paths. In our tests, these needle paths are uniformly chosen in a ± 30 -degree cone around an axis which passes through the targeted needle-placement position on the lung nodule motion path and is along the Z direction of the motion stage (roughly speaking, it is perpendicular to the plane of lung nodule motion). Fig.11 shows a collection of example needle paths which are oriented differently but all end at the same target point where the needle will hit the lung nodule phantom. In the tests, an 18-gauge needle set is used, which has a length of 150mm and consists of a stylet with a diameter of 1.270mm and a cannula with an outer diameter of 0.838mm. The robot is programmed to advance the needle at 564.4mm/second to cross an insertion distance of 150-160mm.

As the outcome of the tests, we measured the needle placement error at a precision of 0.1mm. Out of the 450 trials, the mean error is about 0.4 mm, and the standard deviation is $\ll 0.1$ mm. Error is the root mean square distance of the point of insertion of the needle into the sponge and the center of the ink mark made on the sponge. The current clinical CT-guided needle biopsy procedure usually considers lung nodules with a size >8 mm (with a reported minimum of 4mm [33]). The above positioning accuracy of the robotic needle driving system provide the confidence to biopsy those nodules under respiratory motion, and even biopsy smaller nodules which are not currently considered for needle biopsy.

During the tests, the timing of the robotic needle placement is almost perfect: the robot needle driving is triggered at the beginning of the full exhalation phase; the image processing takes <0.05 second, the needle placement takes <0.29 second, while each respiratory phase lasts 0.4second. Since the needle placement can be accomplished within the respiratory phase where the nodule speed is zero, we can exclude the mismatch in timing between needle advancement and nodule movement as one main cause of the measured needle placement error. Instead, the needle placement error is caused by the combined effect of the spatial errors of robot, motion stage, camera image processing, and manual measurement. Moreover, the vibration of the robot mounting, which is not sufficiently firm, during the robot manipulation, can be a major contributor to the error. Even so, the results show that the robotic needle placement system is able to accurately hit a target that moves like a lung nodule with respiratory motion.

Further testing was done using a skin phantom setup. A skin like material was stretched above the motion stage such that the needle has to pass through the skin and hit the sponge that acts as the target. This test was successful only for perfectly vertical trajectories. For trajectories where the needle is inclined, the biopsy needle was deflected, moving the tip of the needle away from the target ink mark in the sponge.

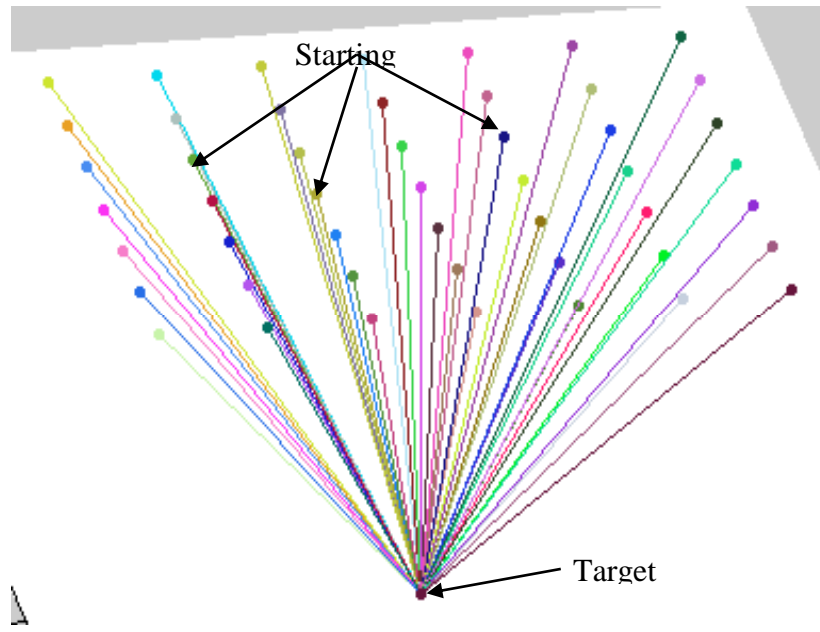


Figure 4.5 Needle paths

Chapter 5. BENDING

This chapter presents a simple way to predict the amount of bending that could be expected in a typical biopsy needle when inserted in to non-homogeneous tissue. This method treats the needle as a cantilever beam and uses basic solid mechanic principles to predict the unknown force distribution acting on the needle inside the tissue. The validity of this method is tested experimentally for known and unknown force distributions.

5.1. Overview of the Needle Bending Problem

Minimally invasive percutaneous procedures have gained popularity in the recent years. Blood/fluid sampling, regional anesthesia, tissue biopsy, abscess drainage, catheter insertion, cryogenic ablation, electrolytic ablation, brachytherapy, neurosurgery, deep brain stimulation and minimally invasive surgeries etc., are commonly performed percutaneous procedures [105]. The effectiveness of these procedures depends on the needle reaching the targeted area. The needle is prevented from reaching the targeted are by tissue deformation and needle bending [97]. It requires skill and experience from the physician to perform these percutaneous procedures.

Most needles bend when inserted into tissue, especially long needles that need to pierce though layers of tissue with different properties. The bending of the needle has been attributed to the geometry of needle tips [98, 99] and the mechanical properties of the tissue [100]. Needles with small diameter and bevel tips have been found to bend more than needles with symmetric tips [101]. While the bending of the bevel tipped needle is attributed to its asymmetry, the bending of conical and triangular needles are attributed to the mechanical properties of the tissue. A pre-bent stylet was suggested to control the bending in [106]. DiMaio et al. [102] developed a

finite element method to model the bending of the needle. This method did not take into account the in-homogeneity of the tissue and requires prior knowledge of mechanical properties of the tissue. A virtual spring model was suggested by Glozman et al. [103], however this method requires real time feedback from a X-ray machine to find the coefficients of the virtual springs. Real time feedbacks from x-rays [103] and ultrasounds [104] have been proposed to solve the needle bending problem. However this is really expensive and exposes the patient to a lot of radiation.

5.2. The Force distribution Approximation method

The method described here predicts the position of the tip of the bent needle based on the observed deflection of the needle outside the body and the reaction forces at the head of the needle. A model of the force distribution experienced by the needle inside the tissue is built. This model is updated periodically and used to predict the position of the needle tip when inserted to the desired depth. This method does not need prior knowledge of the mechanical properties of the tissue and does not need real time feedback from any medical imaging system.

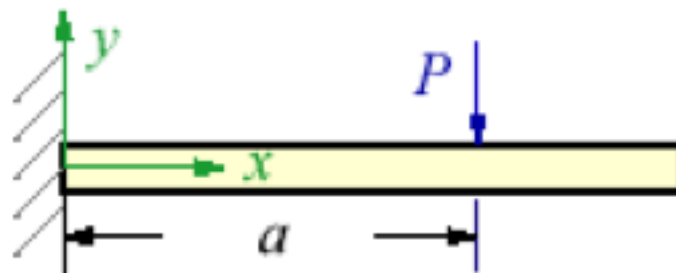


Figure 5.1 Cantilever Beam

The needle is considered as a cantilever beam that is subjected to loading. When a needle is inserted into tissue, forces act upon the needle on its sides. Imbalance in these forces causes bending. This resultant force distribution that causes bending is considered as the load acting on

the cantilever beam. We know that any force distribution can be simplified as a point force. The magnitude of the point force will be equal to the area under the force distribution curve and it will act at the centroid of the area. Whenever any force is applied on a cantilever a reaction force of equal magnitude is felt at the cantilevered end. In our case the cantilevered end is the needle gripper with force sensors capable of measuring the reaction force. The magnitude of the resultant force is found from the reaction at the head of the needle. The direction of the resultant force should be same as the direction of bending. This direction is found from visual feedback on the bending of the needle outside the tissue. Only after the exact direction of the bending is found, the reaction forces from the gripper can be resolved to find the actual magnitude of the total resultant force. Once the direction of the bending is known and the magnitude of the load is found from the reaction at the head of the needle, the bending on the needle is considered as a two-dimensional problem along the plane of bending of the needle as shown in Figure 5.1. Since we observe the bending of the needle outside the body and we already know the magnitude of the reaction force, we can apply equation (1) on any point on the needle and find out the 'EI' and 'a'. EI will be a constant since the Young's modulus and the moment of inertia of the needle do not change. If the EI of the needle is already known we can use the known value.

$$y = \frac{Px^2}{6EI} (\dots\dots\dots (1)$$

Equation (1) is the bending equation of a cantilever beam. Assume that the needle is inserted to a certain known depth into the tissue and there is some bending. The part of the needle inside the tissue is subjected to some unknown distribution of force f(x) that is causing the bending. We need to know this distribution f(x) in order to predict the position of the tip of the needle when inserted to the desired depth. From the reaction at the head of the needle, the magnitude of the

resultant force that is causing the bending can be found. Once the magnitude is known the bent needle outside the tissue is observed to measure the amount of bending. Applying the amount of bending “y” and the magnitude of the force “p” to equation (1) we can find the “EI” of the needle and the point of application of the resultant “a”. With the knowledge of the equivalent point force that is causes the same bending as the force distribution f(x) we try to approximate the function f(x) to make further prediction on the bending of the needle. The area under the curve can be denoted as the integral of the force distribution function as in equations (2).

$$F(x) = \int_a^x f(t)dt = \text{area}$$

$$F'(x) = f(x) \dots\dots\dots(2)$$

$$F'(x) \approx \frac{F(x + \Delta x) - F(x)}{\Delta x} = f(x)$$

F(x) is the point force equivalent of the force distribution and f(x) will a point on the force distribution curve. To keep Δx small the increments in the depth have to be small and the slope of the distribution curve should also be small. Once we have a few values of f(x) i.e. a few points on the force distribution curve, we can fit a curve to find an approximation of the function. Fourier series is used as the standard base onto which the force distribution will be fit. Once the force distribution is found, we can predict the position of the tip of the needle after being inserted to the desired depth. Points on the unknown force distribution curve can be found using equation (2). The needle is inserted into the tissue in small increments, with the knowledge of F(x), Δx and F(x+Δx); points on the curve f(x) are found. Once points on the curve are available, a curve is fit onto those points to find the force distribution function. The Fourier series is used as the base onto which the curve will be fit. The first 5 terms of the Fourier series are considered. So we need at least 6 points on the force distribution curve are required.

This method can be divided into three steps. The first step is to find the “EI” of the needle and the point of application of the force “a”. The magnitude of the resultant force “P” is found from the reaction at the head of the needle. To find EI and ‘a’ we need to know few other points on the deflected needle. These points are collected from the part of the needle outside the tissue. Applying the points to equation (1) we can find the “a” and “EI”. The second step is, finding the distribution of force inside the tissue. This is an iterative process; for each iteration, the needle is inserted one step further into the tissue and a point force equivalent of the force distribution is found. Using equations (2) we can find points on the force distribution curve. Once we have enough points we can fit a curve onto those points to get the force distribution inside the tissue. The third step is to predict the position of the needle tip when inserted to the desired depth, i.e. when the needle is subjected to the entire force distribution. Once the force distribution curve is known, we can predict the position of the tip of the needle using cantilever equations.

5.3. Experimental Testing

The aim of these experiments is to test the validity of the force distribution approximation method. So the needle is subjected to known force distributions. Based on the bending of the needle and the feedback from the sensors in the needle gripper these distributions are approximated. It is difficult to physically apply a force distribution on the needle and measure its deflections. So, the force distribution is converted to an equivalent point force and this point force is applied to the needle. As described earlier, this is a step by step process, so the entire force distribution is not considered at once. The depth by which the needle is advanced for each step is fixed. So the effect of the force distribution for the portion of the needle considered to be inside the tissue is known. This is converted to a point force and applied to the needle. The magnitude and the point of application of these forces are found from the defined force

distribution. These forces are applied on the needle one by one and the bending is observed.



Figure 5.2 Experimental setup.

The needle is positioned horizontally as shown in Figure 5.2. To apply the load we use a motorized test stand, EMS 300 with a force gauge. The test stand is mounted with the force gauge and can be moved up to exert force on the needle. This setup is referred to as the force machine. The Force machine applies known amount of force on the needle in the positive Y direction. A thin thread is tied to the hook of the force gauge. This thread is used to exert the force on the needle to make the point of contact smaller.

The magnitude of the force can be found from the reaction at the head of the needle. The sensors placed on the needle gripper are capable of measuring the reaction force accurately. The output from the sensors is in volts ranging from zero to twenty. The output from the sensors is connected to a data acquisition board and connected to the central computer. Figure 5.3 shows

the program created in LabVIEW to collect the data from the four sensors in the needle gripper. To calibrate the sensors a known force is applied to them and the output is noted. Once the sensors are calibrated the needle is mounted and loaded using the force machine.

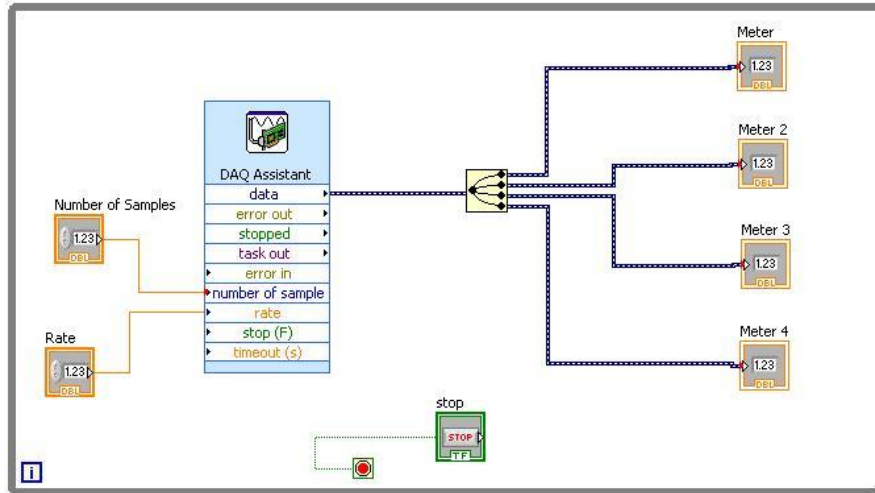


Figure 5.3 Data Acquisition using LabVIEW

By observing the part of the needle that is assumed to be outside the body a curve representing the curvature of the needle is fitted. The position of the tip of the needle is to be found based on this fitted curve. However the curve fitted to the points observed from the part of the needle assumed to be outside the body, do not match the cantilever bending equation. The cantilever bending equation (1) has only third degree and second degree terms. The curve fitted experimentally is more linear. This error is traced back to the strength of the needle gripper. The needle gripper currently being used is not firm enough to perfectly cantilever the needle when being subjected to load. Hence the head of the needle which is supposed to be firmly cantilevered moves when loaded. So the needle does not behave like a cantilever. To avoid this problem the needle is fixed firmly onto a table, and the force machine applies a known load. This eliminates our ability to measure the magnitude of the reaction force from the sensors. However, it has been proved that the magnitudes of the reaction forces can be accurately measured. So the

experiment is continued assuming that the reaction forces are known.

The needle is observed using a camera. To facilitate the process of observing the bending of the needle specific points on the needle are marked using red tape. These points are tracked before and after the application of the load by the camera. Figure 5.4(a). shows the raw image captured by the camera and Figure 5.4(b) the logical image got after being threshold to obtain only the points marked by the red tape. The logical image makes the process of tracking points along the needle easy.

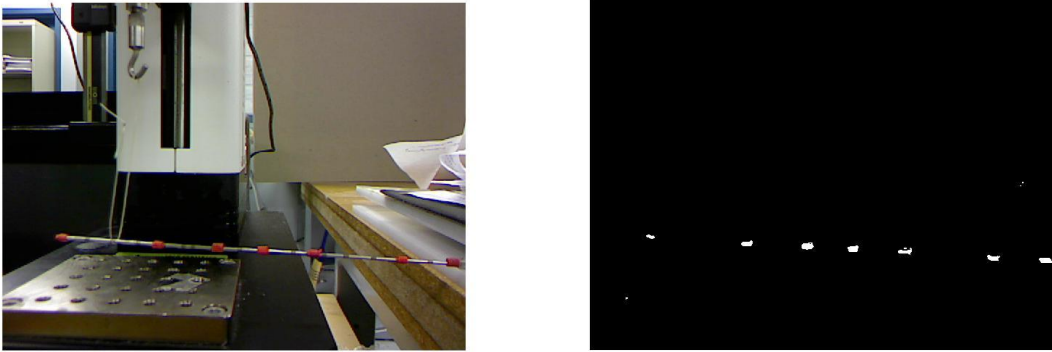


Figure 5.4 Points on needle observed by using camera

The position of each point is tracked separately. The fixed end of the needle is defined as the origin. The positive X axis is assumed to be along the length of the needle and the positive Y axis is assumed to be along the direction of bending. The positions of the points on the needle before and after bending are calculated from the logical images. In the logical image the centroids of the white areas will represent the location of the points. This gives us 6 points, corresponding to the six red tapes on the needle. These six points are fitted onto a third degree polynomial forcing the linear term and the constant term to be zero, so that the resultant equation matches the cantilever equation. Figure 5.5 shows the logical image obtained when the load bends the needle.



Figure 5.5. Bent needle observed using camera

A curve is fitted to the collected points. A pretty close fit is obtained using the Matlab's curve fitting toolbox. " $f(x) = p1*x^3 + p2*x^2 + p3*x + p4$ " is the base equation onto which the points from the cantilever are fixed. As mentioned before the linear and the constant terms are forced to be zero to match this equation with the standard cantilever bending equation. The coefficient got for one particular trial are $p1 = -4.381e-007$, $p2 = 0.0003822$, $p3 = 0$ and $p4 = 0$.

Figure 5.6 shows the graph of a curve that is fitted to the cantilever beam and the equation. The point of application of the force 'a' is also found. Since the length of the needle is known, we can apply that to find the deflection at the tip of the needle.

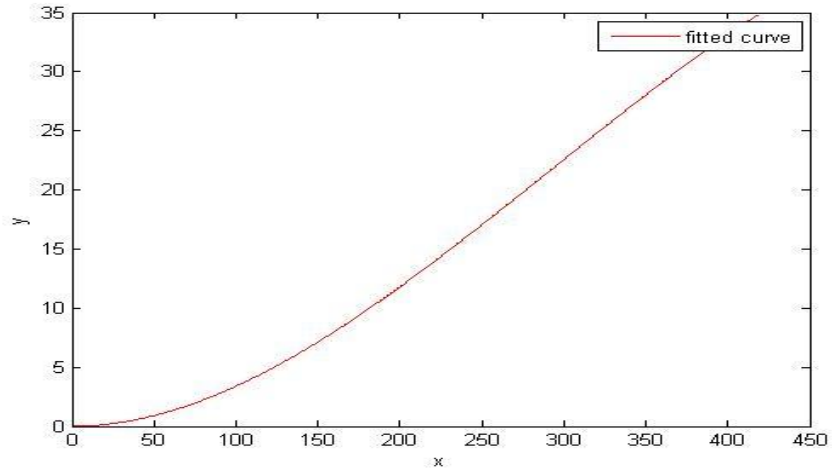


Figure 5.6 Bending of the needle

During the experiment the tip of the needle is hidden from the camera with a small piece of cardboard. Figure 5.7(a) shows the bent needle, with the blue dot indicating the predicted position of the needle tip. The tip of the needle is hidden in the first image, assuming the tip is inserted into the tissue and not visible to the camera. The accuracy of this method can be appreciated from the second image showing the tip of the needle.

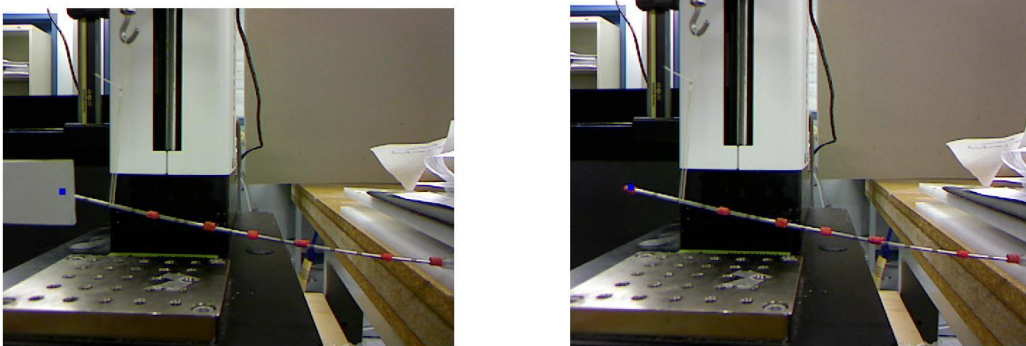


Figure 5.7 Predicted tip of the needle

The accuracy of this part of the experiment is measured as the distance between the predicted tip of the needle and the actual tip of the needle. All units of length have been measured in pixels till this point to reduce the errors due to the calibration of the camera.

However the size of each pixel is calculated now to make more sense of the results. Since the length of the needle is known, the pixel coordinates of the ends of the needle are selected the difference is equated the known length. The length of the needle in pixels is 535 pixels and we know the length is 150 mm. So each pixel is .28mm big. The error measured as the distance between the predicted and the actual needle tip position is 1.5 pixels so the actual error measured in millimeters is .42mm. This error can be reduced by removing the red tapes on the needle. The red tapes are made of rubber and they shrink when heated. They add to the strength of the needle and the Young's modulus of the needle is affected by this. Removing them will reduce the error. Also the cantilevering of the needle is not perfect though the needle is held firmly along the direction of application of the force; there is a little play in the direction perpendicular to it. Firmly cantilevering the needle will reduce the error.

The main aim of the experiment is to find the force distribution inside the tissue. To find that the above described part of the experiment is repeated several times by changing the point of application of the force and the amount of force being applied. This is to simulate the insertion of the needle into the tissue. When the needle is inserted one step further into the tissue, the centroid of the force distribution curve changes and the area under the force curve also changes. Changing the magnitude and the point of application of the force by moving the force machine simulates this. Each time this experiment is repeated, using the equation (2) we find points on the force distribution curve. More the number of trails, the better our estimate of the unknown force distribution function $f(x)$. Again, Matlab's curve fitting toolbox is used to fit a curve to the points. The fitted curve will be the force distribution on the needle and this distribution is extended to the required depth of insertion by extrapolation, to predict the position of the needle tip when inserted completely.

To test the efficiency of this method the following force distributions were defined and then approximated using this method. First a uniformly distributed load is assumed. The distribution is assumed to have a magnitude of 0.01 N/mm. The magnitudes and centroids of the equivalent point force at different stages of insertion of the needle are calculated. It is assumed that the needle is inserted 5 millimeters for each step. So after the first step the total load will be 0.05 and it will act 2.5mm away from the tip of the needle. Similar calculations are carrier out and the needle is loaded with the point forces found from the above said method and the first part of the experiment is repeated. Using equation (2) actual points on the force distribution curve are found and a curve is fitted to these points. The standard form of the curve that is to be fitted is “ $f(x) = a_0 + a_1 \cdot \cos(x \cdot w) + b_1 \cdot \sin(x \cdot w) + a_2 \cdot \cos(2 \cdot x \cdot w) + b_2 \cdot \sin(2 \cdot x \cdot w)$ ” and the coefficients found using Matlab are $a_0 = 0.01$, $a_1 = 4.879e-014$, $b_1 = 1.528e-014$, $a_2 = -1.065e-014$, $b_2 = -7.392e-015$ and $w = 0.0683$.

Figure. 5.8 shows the curves for uniformly distributed load.

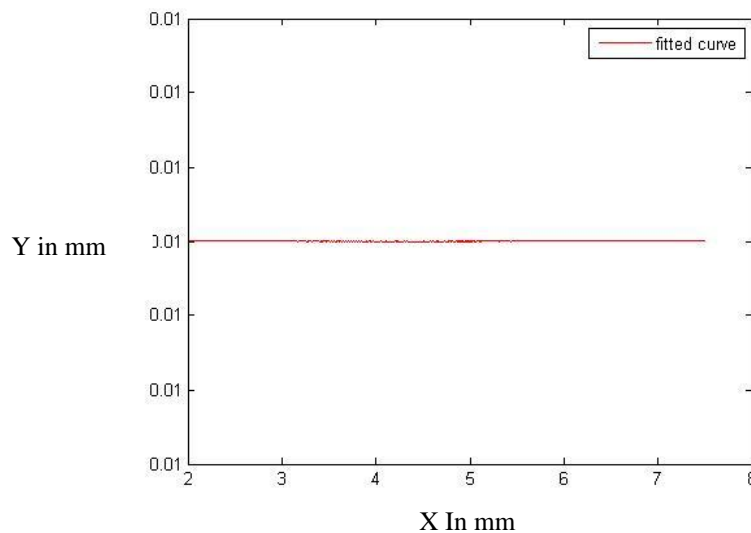


Figure. 5.8. Force distributions curves with equations

Similarly a uniformly varying load is defined and the magnitudes and centroids of the point

forces equivalent are calculated as above. Again the points of the force distribution curve got from using equation(2) are fitted to a generic equation of the form “ $f(x) = a_0 + a_1 \cos(x*w) + b_1 \sin(x*w) + a_2 \cos(2*x*w) + b_2 \sin(2*x*w)$ ”. The coefficients found by fitting a curve onto the points generated by the experiment are $a_0 = 0.0225$, $a_1 = -0.007508$, $b_1 = -0.01904$, $a_2 = -0.002016$, $b_2 = -0.002159$ and $w = 0.0683$. Figure 5.9 shows the curve generated for the uniformly varying load. We can observe the fitted curves have followed the originally assumed load distributions exactly.

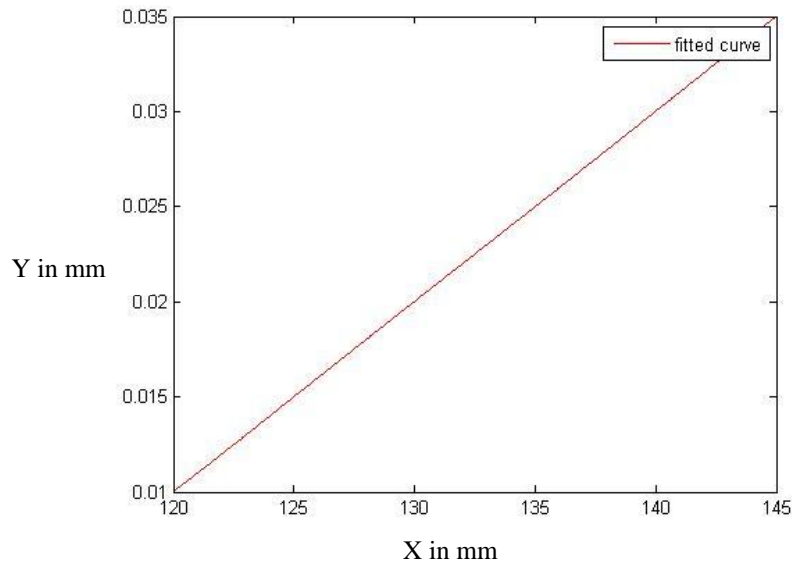


Figure 5.9 Uniformly Varying Force Distribution

Further to test the effectiveness of the force approximation method to trace more complex force distribution a random distribution is assumed and the whole process is repeated. The coefficient values got are $a_0 = -0.6593$, $a_1 = 0.7456$, $b_1 = 0.5441$, $a_2 = -0.08509$, $b_2 = -0.2308$ and $w = -0.04297$. Figure 5.10 shows the force distribution generated. The significance of this curve is that it proves the ability of the generic function to approximate functions that have more than one direction of curvature.

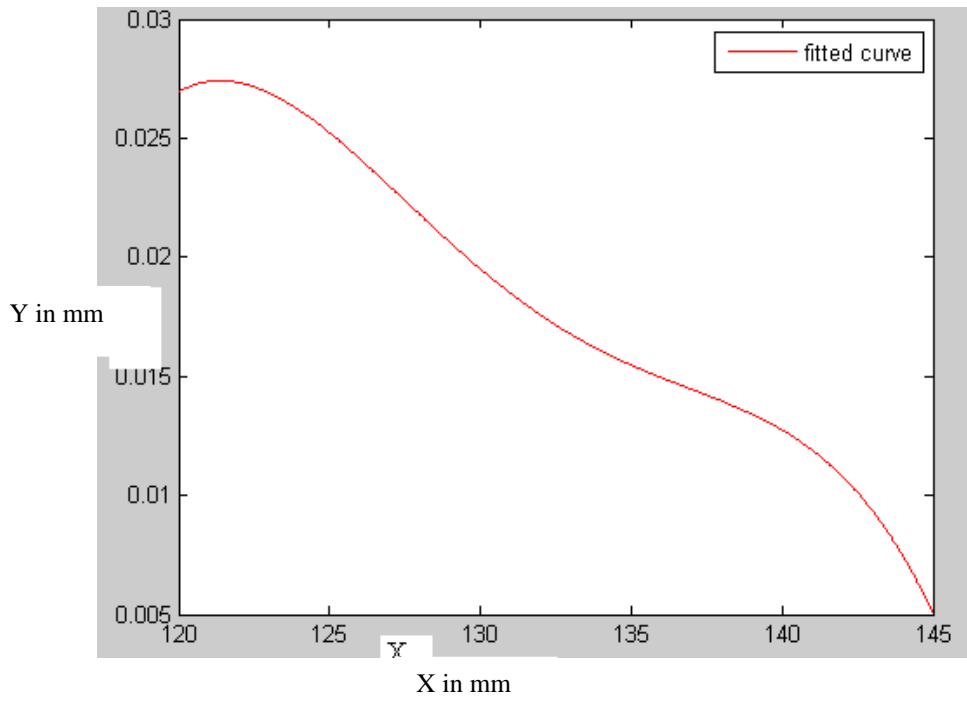


Figure 5.10 Random Force Distribution

Chapter 6. CONCLUSION AND FUTURE WORK

A robot manipulator with a specially-designed effector will place the biopsy needle on a targeted lung nodule according to the patient respiratory motion pattern. CT scans will be taken to model the respiratory motion of the lung nodule, internal structures and skin surface, and for online needle path confirmation.

The proposed CT-guided robotic needle biopsy technique adapts to the patient respiratory motion pattern. The patient respiratory motion model will provide a continuous, real-time guidance to the robotic needle placement process, which will enable accurate needle biopsy of lung nodules on patients who have difficulty in holding their breath. The robotic operation will bring in steady access and precise micro-motion, eliminate the operator-dependent error, e.g. tremor when holding and advancing the needle, and therefore result in high accuracy, reliability and patient safety in needle placement. With the continuous guidance and fast robot motion, the robotic needle biopsy procedure will have a short operation time, which will reduce the occurrence of procedure-induced complications and maximize patient comfort. Moreover, using a robot to deliver the biopsy needle will eliminate the radiation exposure to the clinician who conducts the biopsy procedure. Besides, the concept of robotic needle placement is well applicable to the needle biopsy of lung nodules on patients who can hold their breath, with improved the needle placement accuracy and reduced the procedure duration. In addition, since the proposed technique adapts to the motion of the lung and relevant internal structures, it will provide a new clue to the biopsy and other percutaneous intervention procedures of other moving organs and structures.

As an early-stage study, we have set up an offline robotic experiment system to facilitate the development and evaluation of algorithms for planning and controlling the robot needle

placement process, which consists of the moving lung nodule phantom subsystem, robotic needle manipulation subsystem, and real-time vision feedback subsystem. The preliminary test results show that the proposed robotic needle placement technique allows the biopsy needle to hit a moving target at a high accuracy.

A simple method for predicting the amount of deflection of the biopsy needle was discussed. The method was tested experimentally with satisfactory accuracy. Known force distributions were defined and they were retraced by the force distribution approximation method.

With the ultimate goal of making the proposed CT-guided robotic needle biopsy technique a clinically available technique for biopsying lung nodules and other moving targets. Unlike presently available medical robotic systems the biopsy robot will do the biopsy on its own without the need for human interference. Our next steps of research will focus on the core component techniques:

- 1) *Respiratory motion modeling*: to determine the respiratory motion pattern of the target nodule and potentially interfering organs and the correlation between the internal respiratory motion and skin-surface motion.
- 2) *Needle path planning*: to determine the optimal needle path for hitting the target at the optimal timing and avoiding obstacles.
- 3) *Needle advancement control*: to control the needle placement process optimally and safely based on the respiratory motion model and planned needle path.
- 4) *Needle deflection analysis*: to measure/estimate the needle deflection during the needle placement process and compensate the effect of needle deflection in needle path planning and needle advancement control.

The image processing algorithm described can process 21 frames per second; it can be improved by reducing the image processing load. In the current method the whole image is thresholded to find the location of the fiducial marker. The top left corner of the marker is detected and it represents the position of the marker. So when the left corner is found once, in successive frames a smaller neighborhood of the previous location of the top left corner of the marker could be scanned. The neighborhood should be defined such that it is big enough to keep the top left corner inside the neighborhood even when the marker is moving at its top speed. This would reduce the image processing load significantly. The method of thresholding could be replaced by more edge detection and object tracking algorithms that will be more robust in varying circumstances.

The force approximation method provides a way to predict the bending of the needle. Once the position of the tip of the needle is found out, it has to be corrected. A method to do these corrections has to be developed. When these corrections are made the response of the tissue should be accounted for. So the method should include the factor of tissue deformation in it.

REFERENCES

- [1] Deaths by Cause, Sex and Mortality Stratum, World Health Organization, 2004, http://www.who.int/whr/2004/annex/topic/en/annex_2_en.pdf.
- [2] Cancer, World Health Organization, 2006, <http://www.who.int/mediacentre/factsheets/fs297/en/>.
- [3] Cancer Facts and Figures, American Cancer Society, 2006.
- [4] Lung Cancer Fact Sheet, American Lung Association, 2006, http://www.lungusa.org/site/c.dvLUK9O0E/b.669263/k.6727/Lung_Cancer_Fact_Sheet.htm.
- [5] C. I. Henschke, D. F. Yankelevitz, D. M. Libby, M. W. Pasmantier, J. P. Smith, O. S. Miettinen, “Survival of patients with stage I lung cancer detected on CT screening”, *The New England Journal of Medicine*, 355(17): 1763–1771, 2006.
- [6] H. L. Howe, X. Wu, L. A. Ries, V. Cokkinides, F. Ahmed, A. Jemal, B. Miller, M. Williams, E. Ward, P. A. Wingo, A. Ramirez, B. K. Edwards, “Annual Report to the Nation on the Status of Cancer, 1975-2003”, *Cancer*, 107(8): 1711-1742, 2006.
- [7] J. J. Pagani, “Normal adrenal-glands in small cell lung-carcinoma – CT-guided biopsy”, *American Journal of Roentgenology*, 140(5): 949-951, 1983.
- [8] M. L. Pinstein, R. L. Scott, J. Salazar, “Avoidance of negative percutaneous lung-biopsy using contrast-enhanced CT”, *American Journal of Roentgenology*, 140(2): 265-267, 1983.
- [9] L. B. Haramati, J. H. M. Austin, “Complications after CT-guided needle-biopsy through aerated versus nonaerated lung”, *Radiology*, 181(3): 778-778, 1991.
- [10] E. L. Bressler, J. M. Nelson, “Primary pulmonary-artery sarcoma – diagnosis with CT, MR imaging, and transthoracic needle-biopsy”, *American Journal of Roentgenology*, 159(4): 702-704, 1992.

- [11] G. Raghu, "Interstitial lung disease: a diagnostic approach. Are CT scan and lung biopsy indicated in every patient?", *American Journal of Respiratory and Critical Care Medicine*, 151(3): 909-914, 1995.
- [12] H. Q. Li, P. M. Boiselle, J. A. O. Shepard, B. TrotmanDickenson, T. C. McLoud, "Diagnostic accuracy and safety of CT-Guided percutaneous needle aspiration biopsy of the lung: Comparison of small and large pulmonary nodules", *American Journal of Roentgenology*, 167(1): 105-109, 1996.
- [13] E. A. Kazerooni, F. T. Lim, A. Mikhail, F. J. Martinez, "Risk of pneumothorax in CT-guided transthoracic needle aspiration biopsy of the lung", *Radiology*, 198(2): 371-375, 1996.
- [14] D. F. Yankelevitz, C. I. Henschke, J. H. Koizumi, N. K. Altorki, D. Libby, "CT-guided transthoracic needle biopsy of small solitary pulmonary nodules", *Clinical Imaging*, 21(2): 107-110, 1997.
- [15] N. Hayashi, T. Sakai, M. Kitagawa, T. Kimoto, R. Inagaki, Y. Ishii, S. Noriki, Y. Imamura "CT-guided biopsy of pulmonary nodules less than 3 cm: Usefulness of the spring-operated core biopsy needle and frozen-section pathologic diagnosis", *American Journal of Roentgenology*, 170(2): 329-331, 1998.
- [16] F. Laurent, P. Michel, V. Latrabe, M. T. de Lara, R. Marthan, "Pneumothoraces and chest tube placement after CT-guided transthoracic lung biopsy using a coaxial technique: Incidence and risk factors", *American Journal of Roentgenology*, 172(4): 1049-1053, 1999.
- [17] F. Kodama, T. Ogawa, M. Hashimoto, Y. Tanabe, Y. Suto, T. Kato, "Fatal air embolism as a complication of CT-guided needle biopsy of the lung", *Journal of Computer Assisted Tomography*, 23(6): 949-951, 1999.

- [18] B. L. Connolly, P. G. Chait, D. S. Duncan, G. Taylor, "CT-guided percutaneous needle biopsy of small lung nodules in children", *Pediatric Radiology*, 29(5): 342-346, 1999.
- [19] H. Tsukada, T. Satou, A. Iwashima, T. Souma, "Diagnostic accuracy of CT-guided automated needle biopsy of lung nodules", *American Journal of Roentgenology*, 175(1): 239-243, 2000.
- [20] F. Laurent, V. Latrabe, B. Vergier, P. Michel, "Percutaneous CT-guided biopsy of the lung: Comparison between aspiration and automated cutting needles using a coaxial technique", *Cardiovascular and Interventional Radiology*, 23(4): 266-272, 2000.
- [21] F. Laurent, V. Latrabe, B. Vergier, M. Montaudon, J. M. Vernejous, J. Dubrez, "CT-guided transthoracic needle biopsy of pulmonary nodules smaller than 20 mm: Results with an automated 20-gauge coaxial cutting needle", *Clinical Radiology*, 55(4): 281-287, 2000.
- [22] M. J. Charig, A. J. Phillips, "CT-guided cutting needle biopsy of lung lesions - Safety and efficacy of an out-patient service", *Clinical Radiology*, 55(12): 964-969, 2000.
- [23] K. M. Yeow, L. C. See, K. W. Lui, M. C. Lin, T. C. Y. Tsao, K. F. Ng, H. P. Liu, "Risk factors for pneumothorax and bleeding after CT-guided percutaneous coaxial cutting needle biopsy of lung lesions", *Journal of Vascular and Interventional Radiology*, 12(11): 1305-1312, 2001.
- [24] A. Fukushima, K. Ashizawa, N. Aso, M. Takao, H. Hayashi, K. Nagaoki, I. Sakamoto, K. Hayashi, "CT-guided needle biopsy of the Lung: Factors affecting risk of complications", *Nippon Acta Radiologica*, 61(3): 96-99, 2001.
- [25] M. J. Wallace, S. Krishnamurthy, L. D. Broemeling, S. Gupta, K. Ahrar, F. A. Morello, M. E. Hicks, "CT-guided percutaneous fine-needle aspiration biopsy of small (\leq 1-cm) pulmonary lesions", *Radiology*, 225(3): 823-828, 2002.

- [26] H. Saji, H. Nakamura, T. Tsuchida, M. Tsuboi, N. Kawate, C. Konaka, H. Kato, "The incidence and the risk of pneumothorax and chest tube placement after percutaneous CT-guided lung biopsy - The angle of the needle trajectory is a novel predictor", *Chest*, 121(5): 1521-1526, 2002.
- [27] P. R. Geraghty, S. T. Kee, G. McFarlane, M. K. Razavi, D. Y. Sze, M. D. Dake, "CT-guided transthoracic needle aspiration biopsy of pulmonary nodules: Needle size and pneumothorax rate", *Radiology*, 229(2): 475-481, 2003.
- [28] Y. Ohno, H. Hatabu, D. Takenaka, T. Higashino, H. Watanabe, C. Ohbayashi, K. Sugimura, "CT-guided transthoracic needle aspiration biopsy of small (≤ 20 mm) solitary pulmonary nodules", *American Journal of Roentgenology*, 180(6): 1665-1669, 2003.
- [29] T. Yamagami, S. Iida, T. Kato, O. Tanaka, T. Nishimura, "Combining fine-needle aspiration and core biopsy under CT fluoroscopy guidance: A better way to treat patients with lung nodules?", *American Journal of Roentgenology*, 180(3): 811-815, 2003.
- [30] K. M. Yeow, P. K. Tsay, Y. C. Cheung, K. W. Lui, K. T. Pan, A. S. B. Chou, "Factors affecting diagnostic accuracy of CT-guided coaxial cutting needle lung biopsy: Retrospective analysis of 631 procedures", *Journal of Vascular and Interventional Radiology*, 14(5): 581-588, 2003.
- [31] J. M. Anderson, J. Murchinson, D. Patel, "CT-guided lung biopsy: Factors influencing diagnostic yield and complication rate", *Clinical Radiology*, 58(10): 791-797, 2003.
- [32] A. Priola, S. Novello, S. Priola, M. Longo, A. Cataldi, L. Errico, G. Garofalo, M. Giaj Levra, G. V. Scagliotti, C. Fava, "Factors effecting risk of pneumothorax (PNX) in CT-guided transthoracicneedle biopsy of lung lesions: result of 708 consecutive procedures", *Journal of Thoracic Oncology*, 2(8): S362, 2007.

- [33] E. H. Moore, "Percutaneous Biopsy in Lung Cancer", *Seminars in Roentgenology*, 40(2): 154-170, 2005.
- [34] M. J. Wallace, S. Krishnamurthy, L. D. Broemeling, S. Gupta, K. Ahrar, F. A. Morello, M. E. Hicks, "CT-guided percutaneous fine-needle aspiration biopsy of small (≤ 1 -cm) pulmonary lesions", *Radiology*, 225(3): 823-828, 2002.
- [35] Y. Ohno, H. Hatabu, D. Takenaka, T. Higashino, H. Watanabe, C. Ohbayashi, K. Sugimura, "CT-guided transthoracic needle aspiration biopsy of small (≤ 20 mm) solitary pulmonary nodules", *American Journal of Roentgenology*, 180(6): 1665-1669, 2003.
- [36] S. Gupta, S. Krishnamurthy, L. D. Broemeling, F. A. Morello, M. J. Wallace, K. Ahrar, D. C. Madoff, R. Murthy, M. E. Hicks, "Small (≤ 2 -cm) Subpleural Pulmonary Lesions: Short versus Long-Needle-Path CT-guided Biopsy—Comparison of Diagnostic Yields and Complications", *Radiology*, 234(2): 631-637, 2005.
- [37] T. Neicu, H. Shirato, Y. Seppenwoolde, S. B. Jiang, "Synchronized moving aperture radiation therapy (SMART): average tumor trajectory for lung patients", *Physics in Medicine and Biology*, 48(5): 587-598, 2003.
- [38] J. R. van Sornsen de Koste, F. J. Lagerwaard, M. R. J. Nijssen-Visser, W. J. Graveland, S. Senan, "Tumor location cannot predict the mobility of lung tumors: a 3D analysis of data generated from multiple CT scan", *International Journal of Radiation Oncology, Biology, Physics*, 56(2): 348-354, 2003.
- [39] R. F. Young, "Application of robotics to stereotactic neurosurgery", *Neurological Research*, 9(2): 123-128, 1987.
- [40] H. Fankhauser, D. Glauser, P. Flury, Y. Piguet, M. Epitoux, J. Favre, R. A. Meuli, "Robot for CT-guided stereotactic neurosurgery", *Stereotactic and Functional Neurosurgery*, 63(1-4):

93-98, 1994.

- [41] E. Pisani, E. Montanari, G. Deiana, A. Trinchieri, G. Zanetti, S. Tzoumas, A. Guarneri, R. Sala, A. Rovetta, "Robotized prostate biopsy", *Minimally Invasive Therapy & Allied Technologies*, 4(5-6): 289-291, 1995.
- [42] A. Rovetta, R. Sala, "Execution of robot-assisted biopsies within the clinical context", *Journal of Image Guided Surgery*, 1(5): 280-287, 1995.
- [43] D. Glauser, H. Fankhauser, M. Epitoux, J. L. Hefti, A. Jaccottet, "Neurosurgical robot Minerva: first results and current developments", *Journal of Image Guided Surgery*, 1(5): 266-272, 1995.
- [44] R. Andrews, R. Mah, A. Galvagni, M. Guerreo, R. Papsin, M. Wallace, J. Winters, "Robotic multimodality stereotactic grain tissue identification: Work in progress", *Stereotactic and Functional Neurosurgery*, 68(1-4): 72-79, 1997.
- [45] K. Masamune, L. H. Ji, M. Suzuki, T. Dohi, H. Iseki, K. Takakura, "A newly developed stereotactic robot with detachable drive for neurosurgery", *Lecture Notes in Computer Science*, 1496: 215-222, 1998.
- [46] C. S. Tseng, C. W. Chung, H. H. Chen, S. S. Wang, H. M. Tseng, "Development of a robotic navigation system for neurosurgery", *Medicine Meets Virtual Reality*, 62: 358-359, 1999.
- [47] A. Rovetta, "Tests on reliability of a prostate biopsy telerobotic system", *Medicine Meets Virtual Reality*, 62: 302-307, 1999.
- [48] R. D. Howe, Y. Mastuoka, "Robotics for surgery", *Annual Review of Biomedical Engineering*, 1: 211-240, 1999.
- [49] C. S. Tseng, H. H. Chen, S. S. Wang, H. M. Tseng, "Image-guided robotic navigation

- system for neurosurgery”, *Journal of Robotic Systems*, 17(8): 439-447, 2000.
- [50] W. A. Kaiser, H. Fischer, J. Vagner, M. Selig, “Robotic system for biopsy and therapy of breast lesions in a high-field whole-body magnetic resonance tomography unit”, *Investigative Radiology*, 35(8): 513-519, 2000.
- [51] M. H. Loser, N. Navab, “A new robotic system for visually controlled percutaneous interventions under CT fluoroscopy”, *Lecture Notes in Computer Science*, 1935: 887-896, 2000.
- [52] Y. Koseki, K. Chinzei, N. Koyachi, T. Arai, “Robotic assist for MR-guided surgery using leverage and parallelepiped mechanism”, *Lecture Notes in Computer Science*, 1935: 940-948, 2000.
- [53] K. Chinzei, N. Hata, F. A. Jolesz, R. Kikinis, “MR compatible surgical assist robot: System integration and preliminary feasibility study”, *Lecture Notes in Computer Science*, 1935: 921-930, 2000.
- [54] K. Chinzei, K. Miller, “Towards MRI guided surgical manipulator”, *Medical Science Monitor*, 7(1): 153-163, 2001.
- [55] J. A. Cadeddu, D. Stoianovici, R. N. Chen, R. G. Moore, L. R. Kavoussi, “Stereotactic mechanical percutaneous renal access”, *Journal of Endourology*, 12(2): 121-125, 1998.
- [56] J. A. Cadeddu, A. Bzostek, S. Screiner, A. Barnes, W. Roberts, J. Anderson, R. Taylor, L. Kavoussi, “A robotic system for percutaneous renal access”, *Journal of Urology*, 158: 1589-1593, 1997.
- [57] J. Shah, S. Mackay, T. Rockall, J. Vale, A. Darzi, “‘Urobotics’: robots in urology”, *BJU International*, 88(4): 313-320, 2001.
- [58] J. Yanof, J. Haaga, P. Klahr, C. Bauer, D. Nakamoto, A. Chaturvedi, R. Bruce, “CT-

integrated robot for interventional procedures: preliminary experiment and computer-human interfaces”, *Computer Aided Surgery*, 6(6): 353-359, 2001.

- [59] K. Masamune, G. Fichtinger, A. Patriciu, R. Susil, R. H. Taylor, L. R. Kavoussi, J. H. Anderson, I. Sakuma, T. Dohi, D. Stoianovici, “System for robotically assisted percutaneous procedures with computed tomography guidance”, *Computer Aided Surgery*, 6(6): 370-383, 2001.
- [60] G. Fichtinger, T. L. DeWeese, A. Patriciu, A. Tanacs, D. Mazilu, J. H. Anderson, K. Masamune, R. H. Taylor, D. Stoianovici, “System for robotically assisted prostate biopsy and therapy with intraoperative CT guidance”, *Academic Radiology*, 9(1): 60-74, 2002.
- [61] M. Y. Shi, H. Liu, G. Tao, “A stereo-fluoroscopic image-guided robotic biopsy scheme”, *IEEE Transactions on Control Systems Technology*, 10(3): 309-317, 2002.
- [62] S. B. Solomon, A. Patriciu, M. E. Bohlman, L. R. Kavoussi, D. Stoianovic, “Robotically driven interventions: A method of using CT fluoroscopy without radiation exposure to the physician”, *Radiology*, 225(1): 277-282, 2002.
- [63] G. Fichtinger, A. Krieger, R. C. Susil, A. Tanacs, L. L. Whitcomb, E. Atalar, “Transrectal prostate biopsy inside closed MRI scanner with remote actuation, under real-time image guidance”, *Lecture Notes in Computer Science*, 2488: 91-98, 2002.
- [64] A. Felden, J. Vagner, A. Hinz, H. Fischer, S. O. R. Pfleiderer, J. R. Reichenbach, W. A. Kaiser, “ROBITOM-robot for biopsy and therapy of the mamma”, *Biomedizinische Technik*, 47 Supplement Part 1: 2-5, 2002.
- [65] J. J. DeRose, D. G. Swistel, A. Safavi, C. P. Connery, R. C. Ashton, “Mediastinal mass evaluation using advanced robotic techniques”, *Annals of Thoracic Surgery*, 75(2): 571-573, 2003.

- [66] K. Chinzei, S. K. Warfield, N. Hata, C. M. C. Tempany, F. A. Jolesz, R. Kikinis, “Planning, simulation and assistance with intraoperative MRI”, *Minimally Invasive Therapy & Allied Technologies*, 12(1-2): 59-64, 2003.
- [67] S. O. R. Pfleiderer, J. R. Reichenbach, T. Azhari, C. Marx, A. Malich, A. Schneider, J. Vagner, H. Fischer, W. A. Kaiser, “A manipulator system for 14-gauge large core breast biopsies inside a high-field whole-body MR scanner”, *Journal of Magnetic Resonance Imaging*, 17(4): 493-498, 2003.
- [68] D. Stoianovici, K. Cleary, A. Patriciu, D. Mazilu, A. Stanimir, N. Craciunoiu, V. Watson, L. Kavoussi, “AcuBot: A robot for radiological interventions”, *IEEE Transactions on Robotics and Automation*, 19(5): 927-930, 2003.
- [69] P. W. A. Willems, H. J. Noordmans, L. M. P. Ramos, M. J. B. Taphoorn, J. W. B. van der Sprenkel, M. A. Viergever, C. A. F. Tulleken, “Clinical evaluation of stereotactic brain biopsies with an MKM-mounted instrument holder”, *Acta Neurochirurgica*, 145(10): 889-897, 2003.
- [70] K. Cleary, V. Watson, D. Lindisch, A. Patriciu, D. Mazilu, D. Stoianovici, “Robotically assisted interventions: Clinical trial for spinal blocks”, *Lecture Notes in Computer Science*, 2879: 963-964, 2003.
- [71] G. Kronreif, M. Furst, J. Kettenbach, M. Figl, R. Hanel, “Robotic guidance for percutaneous interventions”, *Advanced Robotics*, 17(6): 541-560, 2003.
- [72] J. Hong, T. Dohi, M. Hashizume, K. Konishi, N. Hata, “An ultrasound-driven needle-insertion robot for percutaneous cholecystostomy”, *Physics in Medicine and Biology*, 49(3): 441-455, 2004.
- [73] Z. P. Wei, G. Wan, L. Gardi, G. Mills, D. Downey, A. Fenster, “Robot-assisted 3D-TRUS

- guided prostate brachytherapy: System integration and validation”, *Medical Physics*, 31(3): 539-548, 2004.
- [74] B. T. Larson, A. G. Erdman, N. V. Tsekos, E. Yacoub, P. V. Tsekos, L. G. Koutlas, “Design of an MRI-compatible robotic stereotactic device for minimally invasive interventions in the breast”, *Journal of Biomechanical Engineering-Transactions of the ASME*, 126(4): 458-465, 2004.
- [75] E. Taillant, J. C. Avila-Vilchis, C. Allegrini, I. Bricault, P. Cinquin, “CT and MR compatible light puncture robot: Architectural design and first experiments”, *Lecture Notes in Computer Science*, 3217: 145-152, part 2, 2004.
- [76] K. Cleary, V. Watson, D. Lindisch, R. H. Taylor, G. Fichtinger, S. Xu, C. S. White, J. Donlon, M. Taylor, A. Patriciu, D. Mazilu, D. Stoianovici, “Precision placement of instruments for minimally invasive procedures using a "Needle Driver" robot”, *International Journal of Medical Robotics and Computer Assisted Surgery*, 1(2): 40-47, 2005.
- [77] J. Kettenbach, G. Kronreif, M. Figl, M. Furst, W. Birkfellner, R. Hanel, W. Ptacek, H. Bergmann, “Robot-assisted biopsy using computed tomography-guidance - Initial results from in vitro tests”, *Investigative Radiology*, 40(4): 219-228, 2005.
- [78] J. Kettenbach, G. Kronreif, M. Figl, W. Birkfellner, R. Hanel, H. Bergmann, “Robot-assisted biopsy using ultrasound guidance: initial results from in vitro tests”, *European Radiology*, 15(4): 765-771, 2005.
- [79] S. J. Haker, R. V. Mulkern, J. R. Roebuck, A. S. Barnes, S. Dimaio, N. Hata, C. M. C. Clare, “Magnetic resonance-guided prostate interventions”, *Magnetic Resonance Imaging*, 16(5): 355-368, 2005.
- [80] G. Fichtinger, E. C. Burdette, A. Tanacs, A. Patriciu, D. Mazilu, L. L. Whitcomb, D.

- Stoianovici, "Robotically assisted prostate brachytherapy with transrectal ultrasound guidance - Phantom experiments", *Brachytherapy*, 5(1): 14-26, 2006.
- [81] M. Muntener, A. Patriciu, D. Petrisor, D. Mazilu, H. Bagga, L. Kavoussi, K. Cleary, D. Stoianovici, "Magnetic resonance imaging compatible robotic system for fully automated brachytherapy seed placement", *Urology*, 68(6): 1313-1317, 2006.
- [82] M. E. Rentschler, J. Dumpert, S. R. Platt, S. M. Farritor, D. Oleynikov, "Mobile in vivo biopsy and camera robot", *Proceedings 2006 IEEE International Conference on Robotics and Automation*, 4155-4160, 2006.
- [83] S. P. DiMaio, S. Pieper, K. Chinzei, N. Hata, E. Balogh, G. Fichtinger, C. M. Tempany, R. Kikinis, "Robot-assisted needle placement in open-MRI: system architecture, integration and validation", *Studies in Health Technology and Informatics*, 119: 126-131, 2006.
- [84] Y. Yu, T. Podder, Y. Zhang, W. S. Ng, V. Misic, J. Sherman, L. Fu, D. Fuller, E. Messing, D. Rubens, J. Strang, R. Brasacchio, "Robot-assisted prostate brachytherapy", *Lecture Notes in Computer Science*, 4190: 41-49, 2006.
- [85] L. Phee, J. Yuen, D. Xiao, C. F. Chan, H. Ho, C. H. Thng, P. H. Tan, C. Cheng, W.S. Ng, "Ultrasound guided robotic biopsy of the prostate", *International Journal of Humanoid Robotics*, 3(4): 463-483, 2006.
- [86] S. P. DiMaio, S. Pieper, K. Chinzei, N. Hata, S. J. Haker, D. F. Kacher, G. Fichtinger, C. M. Tempany, R. Kikinis, "Robot-assisted needle placement in open MRI: system architecture, integration and validation", *Computer Aided Surgery*, 12(1): 15-24, 2007.
- [87] C. S. Tseng, C. C. Huang, C. S. Chen, "Development of an image-guided robotic system for surgical positioning and drilling", *Robotica*, 25: 375-383, Part 3, 2007.
- [88] S. Zangos, K. Eichler, A. Thalhammer, J. U. Schoepf, P. Costello, C. Herzog, M. G. Mack,

- T. J. Vogl, "MR-guided interventions of the prostate gland", *Minimally Invasive Therapy & Allied Technologies*, 16(4): 222-229, 2007.
- [89] D. Stoianovici, D. Song, D. Petrisor, D. Ursu, D. Mazilu, M. Mutener, M. Schar, A. Patriciu, "'MRI Stealth" robot for prostate interventions", *Minimally Invasive Therapy & Allied Technologies*, 16(4): 241-248, 2007.
- [90] G. S. Fischer, S. P. DiMaio, I. Iordachita, G. Fichtinger, "Robotic assistant for transperineal prostate interventions in 3T closed MRI", *Lecture Notes in Computer Science*, 4791: 425-433, 2007.
- [91] J. Whitman, M. P. Fronheiser, N. M. Ivancevich, S. W. Smith, "Autonomous surgical robotics using 3-D ultrasound guidance: Feasibility study", *Ultrasonic Imaging*, 29(4): 213-219, 2007.
- [92] M. Muntener, A. Patriciu, D. Petrisor, M. Schar, D. Ursu, D. Y. Song, D. Stoianovici, "Transperineal prostate intervention: Robot for fully automated MR Imaging - System description and proof of principle in a Canine model", *Radiology*, 247(2): 543-549, 2008.
- [93] V. G. Mallapragada, and N. Sarkar, "Robot-assisted real-time tumor manipulation for breast biopsy", *IEEE Transactions on Robotics*, 25(2) : 316-324, 2009.
- [94] K. Liang, A. J. Rogers, E. D. Light, D. von Allmen, and S. W. Smith, "Three-dimensional ultrasound guidance of autonomous robotic breast biopsy : feasibility study ", *Ultrasound in Medicine and Biology*, 36(1) : 173-177, 2010.
- [95] Z. Neubach, and M. Shoham, "Ultrasound-guided robot for flexible needle steering", *IEEE Transactions on Biomedical Engineering*, 57(4) : 799-805, 2010.
- [96] Y. L. Park, S. Elayaperumal, B. Daniel, S. C. Ryu, M. Shin, J. Savall, R. J. Black, B. Moslehi, and M. R. Cutkosky, "Real-time estimation of 3-D needle shape and deflection for

- MRI-guided interventions", IEEE/ASME Transactions on Mechatronics, 15(6) : 906-915, 2010.
- [97] Niki Abolhassani, Rajni Patel, Mehrdad Moallem, "needle insertion into soft tissue: A survey", Medical Engineering and Physics 29(2007) 413-431.
- [98] Kataoka H, et al. A model for relations between needle deflection, force, and thickness on needle insertion. In : Proceedings of the medical image computing and computer-assisted intervention (MICCAI). 2001. P. 966-74.
- [99] Alterovitz R, et al. Planning for steerable bevel-tip needle insertion through 2D soft tissues with obstacles. In : Proceedings of the IEEE international conference on robotics and automation (ICRA). 2005. P. 1652-7.
- [100] Taschereau R, et al. Seed misplacement and stabilizing needles in transperineal permanent prostate implants. Radiother oncol 2000;55 :59-63.
- [101] Okamura AM, et al. Force modeling for needle insertion into soft tissue. IEEE Trans Biomed Eng 2004 ;51(10) :1707-16.
- [102] Simon DiMaio, Modelling, Simulation and Planning of Needle Motion in Soft Tissues, Ph.D dissertation, Univ. British Columbia, B.C., Canada, 2003.
- [103] Daniel Glozman and Moshe Shoham, Image-Guided Robotic Flexible Needle Steering, IEEE transactions on robotics, vol. 23, No. 3, June 2007.
- [104] Zipi Neubach and Moshe Shoham, Ultrasound-Guided robot for flexible needle steering, IEEE transactions on biomedical engineering, vol. 57, No. 4, April 2010.
- [105] Simon P. DiMaio, Septimiu E. Salcudean, Interactive Simulation of Needle Insertion Models, IEEE Transaction of Biomedical Engineering, VOL. 52, NO. 7, JULY 2005 1167
- [106] Stephen Okazawa, Richelle Ebrahimi, Jason Chuang, Septimiu E. Salcudean, Robert

Rohling, Hand-Held Steerable Needle Device, IEEE/ASME Transaction on Mechatronics,
VOL. 10, NO. 3, JUNE 2005 285

[107] <http://www.jefferson.edu/jmc/radiology/divisions/cardiothoracic/services.cfm>